The Astrophysical Journal, 797:126 (19pp), 2014 December 20 doi:10.1088/0004-637X/797/2/126

A CRITICAL LOOK AT THE MASS–METALLICITY–STAR FORMATION RATE RELATION IN THE LOCAL UNIVERSE. I. AN IMPROVED ANALYSIS FRAMEWORK AND CONFOUNDING SYSTEMATICS

Samir Salim[1], Janice C. Lee[2,8], Chun Ly[3,9], Jarle Brinchmann[4], Romeel Davé[5], Mark Dickinson[6], John J. Salzer[1], and Stéphane Charlot[7]
[1] Department of Astronomy, Indiana University, Bloomington, IN 47404, USA; salims@indiana.edu
[2] Space Telescope Science Institute, Baltimore, MD 21218, USA
[3] NASA Goddard Space Flight Center, Greenbelt, MD 20771, USA
[4] Leiden Observatory, Leiden University, NL-2300 RA Leiden, The Netherlands
[5] University of the Western Cape, Bellville, Cape Town 7535, South Africa
[6] National Optical Astronomy Observatory, Tucson, AZ 85719, USA
[7] Institut d'Astrophysique de Paris, CNRS, F-75014 Paris, France
Received 2014 September 29; accepted 2014 November 9; published 2014 December 8

ABSTRACT

It has been proposed that the (stellar) mass–(gas) metallicity relation of galaxies exhibits a secondary dependence on star formation rate (SFR), and that the resulting M_*–Z–SFR relation may be redshift-invariant, i.e., "fundamental." However, conflicting results on the character of the SFR dependence, and whether it exists, have been reported. To gain insight into the origins of the conflicting results, we (1) devise a non-parametric, astrophysically motivated analysis framework based on the offset from the star-forming ("main") sequence at a given M_* (relative specific SFR); (2) apply this methodology and perform a comprehensive re-analysis of the local M_*–Z–SFR relation, based on SDSS, *GALEX*, and *WISE* data; and (3) study the impact of sample selection and of using different metallicity and SFR indicators. We show that metallicity is anti-correlated with specific SFR regardless of the indicators used. We do not find that the relation is spurious due to correlations arising from biased metallicity measurements or fiber aperture effects. We emphasize that the dependence is weak/absent for massive galaxies ($\log M_* > 10.5$), and that the overall scatter in the M_*–Z–SFR relation does not greatly decrease from the M_*–Z relation. We find that the dependence is stronger for the highest SSFR galaxies above the star-forming sequence. This two-mode behavior can be described with a broken linear fit in 12+log(O/H) versus log (SFR/M_*), at a given M_*. Previous parameterizations used for comparative analysis with higher redshift samples that do not account for the more detailed behavior of the local M_*–Z–SFR relation may incorrectly lead to the conclusion that those samples follow a different relationship.

Key words: galaxies: abundances – galaxies: evolution – galaxies: fundamental parameters

Online-only material: color figures

1. INTRODUCTION

The chemical enrichment of galaxies and its change through cosmic time represents one of the key aspects of efforts to arrive at a comprehensive picture of galaxy evolution. Therefore, it is of particular importance that there may exist a relation that connects the gas-phase metal abundance (Z, "metallicity"), the stellar mass of the galaxy (M_*), and its current star formation rate (SFR; Ellison et al. 2008), and that this relation may be redshift-independent, or "fundamental" (hence, "fundamental metallicity relation," or FMR; Mannucci et al. 2010), even though each of the quantities itself evolves for a given galaxy. Despite an impressive amount of work carried out in recent years, there remain fundamental uncertainties concerning the empirical properties of the M_*–Z–SFR relation (Yates et al. 2012; Andrews & Martini 2013), its redshift invariance (e.g., Maier et al. 2014; Steidel et al. 2014) and even whether it exists (Sánchez et al. 2013). This paper explores how the choice and treatment of the observational data affect the perceived character of the M_*–Z–SFR relation, and presents methodological recommendations for a consistent approach to study it and some findings based on the application of this methodology.

The M_*–Z–SFR relation represents an extension of the mass–metallicity (M_*–Z) relation (MZR). MZR was first studied in a small sample of irregular galaxies (Lequeux et al. 1979), and was later firmly established using much larger samples from the Sloan Digital Sky Survey (SDSS) spectroscopic survey (Tremonti et al. 2004, hereafter T04). T04 found MZR to be more fundamental then the previously studied luminosity–metallicity relations (e.g., Garnett 2002; Lee et al. 2004; Salzer et al. 2005). The sense of the MZR is that more massive galaxies have, on average, higher metallicities. The observed scatter of MZR (∼0.1 dex in metallicity) is usually described as "tight," although it should be kept in mind that the full range of metallicities between gas-rich dwarfs ($\log M_* < 8$)[10] and the most massive star-forming (SF) galaxies ($\log M_* \approx 11$) is less than a decade (Andrews & Martini 2013).

Subsequently, building on efforts to study non-local luminosity–metallicity relation (e.g., Kobulnicky & Kewley 2004), the MZR was observed at intermediate redshifts (e.g., Savaglio et al. 2005; Cowie & Barger 2008; Lamareille et al. 2009; Zahid et al. 2011; Cresci et al. 2012; Pérez-Montero et al. 2013; Stott et al. 2013; Ly et al. 2014; de los Reyes et al. 2014) and is also starting to be measured at higher redshifts ($z \gtrsim 1.6$), either from direct observations (Maiolino et al. 2008; Zahid et al. 2014b; Troncoso et al. 2014; Steidel et al. 2014; Maier et al. 2014), stacked spectra (Erb et al. 2006; Henry et al. 2013;

[8] Visiting Astronomer, Spitzer Science Center, Caltech, Pasadena, CA 91125, USA.
[9] NASA Postdoctoral Fellow.
[10] Masses are expressed in units of solar mass ($M_\odot$).

Cullen et al. 2014; Yabe et al. 2014), or by exploiting gravitational lensing (Richard et al. 2011; Christensen et al. 2012; Wuyts et al. 2012; Belli et al. 2013; Yuan et al. 2013). In addition to observational challenges, with some of the diagnostic lines redshifted into the near-infrared region, non-local studies have to contend with the changing characteristics of the interstellar medium (ISM; Nakajima & Ouchi 2014; Steidel et al. 2014) and the increased uncertainties regarding the removal of galaxies in which active galactic nuclei contribute to ionization (Kewley et al. 2013; Juneau et al. 2014) and sample selection effects (Juneau et al. 2014). Nevertheless, the general consensus is that average metallicities at a given mass were lower at higher redshifts. Note that for a given galaxy the evolution in metallicity is even greater than the offset between MZRs because the galaxies we see today had a smaller mass in the past.

The search for secondary dependencies of MZR can be traced back to T04, who remarked that the scatter in MZR is approximately twice the estimated error in metallicity, suggesting that other galaxy properties may contribute to it. They found mass-dependent MZR residuals with respect to the mass surface density, but not with respect to the Hα equivalent width, a rough proxy for specific star formation rate (SSFR = SFR/M_*). Subsequently, also using SDSS but with different method of deriving metallicities, Ellison et al. (2008) found that MZR residuals at a given mass do depend on the SSFR and even more strongly on galaxy's physical size. Both effects were found to be more pronounced at lower masses. Mannucci et al. (2010, hereafter M10) introduced an analytical form for M_*–Z–SFR relation, and more importantly, proposed that the M_*–Z–SFR relation, unlike the MZR, does not evolve with redshift (hence, it is "fundamental"). Thus, MZRs at high redshift simply represent slices of the M_*–Z–SFR relation that can be defined with the local data. M10 also found a projection of the M_*–Z–SFR relation along the axis that lies in the M_*–SFR plane that minimizes the scatter in metallicity compared to the MZR projection. A similar concept sharing the idea of tying together MZRs at different redshifts was concurrently put forward by Lara-López et al. (2010, hereafter LL10).

The idea of a fundamental relation was foreshadowed by Hoopes et al. (2007), who showed that UV luminous compact galaxies, which may represent local Lyman-break galaxy (LBG) analogs, lie on a MZR that is offset from the general MZR toward lower metallicities. They noted that the MZR of UV luminous compact galaxies resembles the $z \sim 0.7$ MZR of Savaglio et al. (2005) in terms of the magnitude of the offset from the local MZR and even the fact that the offset was greater for low-mass galaxies. The invariant aspect of the M_*–Z–SFR relation was considered, but dismissed by Ellison et al. (2008) because they concluded that for high-redshift galaxies, the effect of higher SSFRs would be mostly countered by the effect of high-redshift galaxies being smaller (size was found by these authors to be a stronger driver of metallicity dependence). However, nearly all subsequent studies have only considered the effect of the evolving SFRs, but not also of the size.

The existence of M_*–Z–SFR relation and its possible fundamental aspect were quickly adopted, and theoretical models, both analytical (e.g., Lilly et al. 2013) and numerical (e.g., Davé et al. 2011), were developed to explain it (see Section 5). FMR has even been used as a assumption to yield other predictions (Peeples & Somerville 2013). Furthermore, there are numerous efforts to detect secondary dependencies even at higher redshifts (e.g., Cresci et al. 2012; Zahid et al. 2014b; Wuyts et al. 2014; Steidel et al. 2014; Maier et al. 2014; de los Reyes et al. 2014). Nevertheless, the observational status of the M_*–Z–SFR relation and its exact character are currently unclear even in the local universe where the data are most abundant. For example, in their study of SDSS samples, Yates et al. (2012) find that the anti-correlation between SFR and metallicity at a given mass is only present at lower masses ($\log M_* \lesssim 10.2$), but then *reverses*, so that the metallicity is *higher* for high-SFR galaxies, contradicting the results of M10. More disturbingly, Sánchez et al. (2013) find no dependence of metallicity on SFR at all in their sample of local galaxies with spatially resolved metallicities. In contrast, Andrews & Martini (2013), by measuring direct metallicities on stacked SDSS spectra, find not only that metallicity is anti-correlated with SFR at all masses, but that this dependence is two to three times stronger than that found by M10.

There are also open questions regarding what fraction of metallicity scatter can be accounted for by allowing the SFR dependence, with estimates ranging from very moderate (Ellison et al. 2008; Pérez-Montero et al. 2013) to quite substantial (Mannucci et al. 2010). Finally, the existence of another "second" parameter on which metallicity may depend, the galaxy size, has received relatively little attention despite the initial claims that it is even more important than the dependence on SFR (Ellison et al. 2008).

To achieve a solid understanding of the process of chemical enrichment and be able to interpret theoretical predictions, one first needs to understand the root causes of the discrepant results mentioned. Therefore, this paper will explore the uncertainties regarding the character and the existence of the dependence of metallicity on secondary parameters resulting from different methods of measuring metallicity and SFR. Metallicity determinations have a number of well-known difficulties—both practical and theoretical (e.g., Kewley & Ellison 2008; Andrews & Martini 2013), so it is only natural that may affect the characterization of the M_*–Z–SFR relation. Additional systematics may arise from the fact that SDSS is limited to the use of fiber spectroscopy, which samples only the central regions of galaxies (Sánchez et al. 2013). Star formation indicators are similarly subject to a number of caveats, including uncertainties in calibrations, the types of populations used as tracers, and the dust corrections (e.g., Brinchmann et al. 2004; Salim et al. 2007, 2009; Lee et al. 2009, 2011; Kennicutt & Evans 2012; Calzetti 2013). Furthermore, all of the previous work in SDSS used SFR estimates that are based on some of the same emission lines measurements that are used to derive metallicities, raising concerns about spurious correlations (Lilly et al. 2013). The paper will also address possible biases arising from sample definitions (e.g., de los Reyes et al. 2014), and will revisit the questions of the metallicity scatter and of the secondary dependence of metallicity on galaxy size.

The present study will focus on characterizing the M_*–Z–SFR relation and, more specifically, on verifying the existence of the SFR dependence (i.e., $Z(M_*, \mathrm{SFR})$) in the *local universe* ($z \sim 0.1$). To accomplish these goals, we introduce an intuitive and physically motivated framework that does not pre-suppose a particular parameterization of this relation. The proposed framework can also be naturally applied to establish whether the M_*–Z–SFR relation is epoch-invariant, i.e., whether FMR is indeed fundamental. Note that the question of the existence of FMR (the constancy of M_*–Z–SFR relation) is separate from the question of the existence of $Z(M_*, \mathrm{SFR})$ at any given redshift (Maier et al. 2014). Both of these questions, the FMR and $Z(M_*, \mathrm{SFR})$ at $z \sim 2.3$, will be addressed in a subsequent work (S. Salim et al. 2015, in preparation).

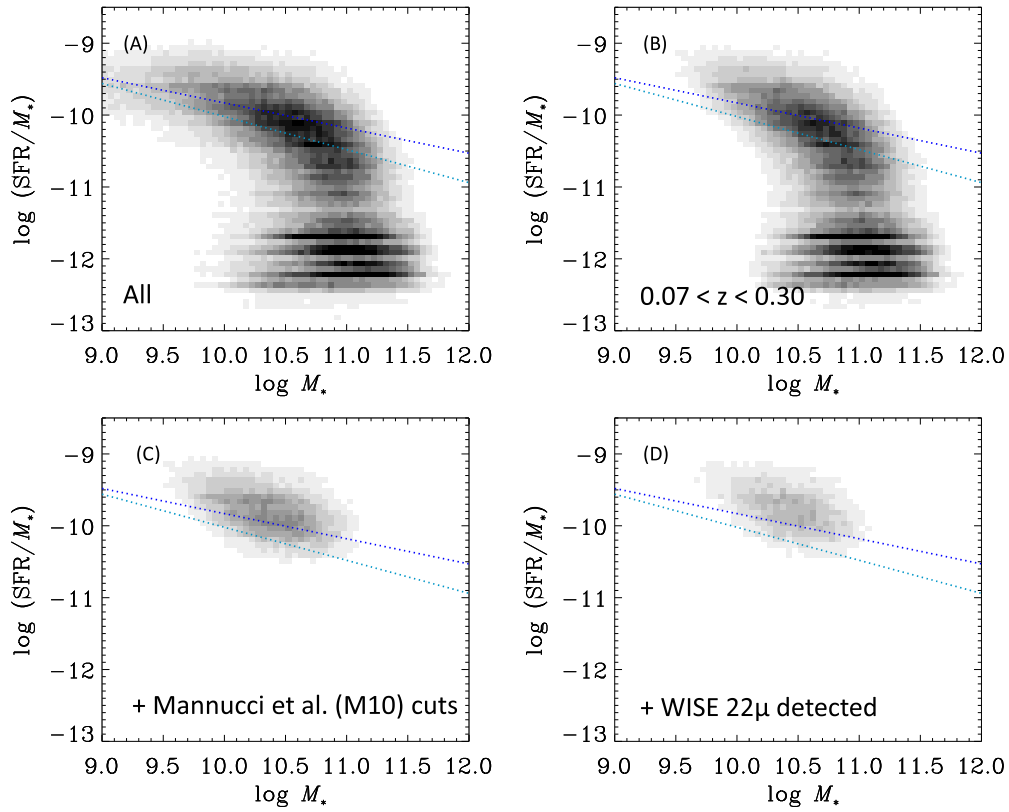

Figure 1. Distribution of specific star formation rates (SFR/M_*) and stellar masses (M_*) illustrating the effects of sample cuts and detection limits. Panel (A) shows the sample (galaxies in the MPA/JHU SDSS DR7 catalog) prior to any cuts. Panel (B) shows the effects of applying the Mannucci et al. (2010, M10) redshift cuts. Panel (C) shows our final "M10-like sample," where we have applied cuts that select star-forming galaxies with strong Hα detection and remove discrepant metallicities, following M10. In our analysis we will also use an *augmented* sample (plot not shown), which practically eliminates low-redshift limit as long as at least 10% of mass is contained in the fiber. Panel (D) shows galaxies from the final M10-like sample (panel (C)) that have detections in *WISE W*4 band (22 μm). A given shade of grayscale represents the same number of galaxies in every panel. Dotted lines show the location of the star-forming sequence according to Salim et al. (2007) ($\beta = -0.35$, upper line) and Salim & Lee (2012) ($\beta = -0.46$, lower line). SSFRs used in this plot come from the UV/optical SED fitting (but the sample is still only optically selected, see Section 2.3), so no biases in the SSFR–M_* plane are introduced.

(A color version of this figure is available in the online journal.)

Throughout the paper we will use two-dimensional representations of familiar quantities, as those are much more readily comprehended than the three-dimensional representations. Striving to make the analysis as intuitive as possible, we will be presenting only two types of plots: mass versus metallicity, and metallicity versus the relative specific SFR (for galaxies of a certain mass).

In Section 2, we present the data used in the study, define the samples, and detail how different measurements were made. In Section 3, we motivate and lay out the non-parametric analysis framework that we will use in the rest of the paper, and explore the character of $Z(M_*, \mathrm{SFR})$ using a variety of SFR and metallicity measurements. In Section 4, we apply our methodology in order to address some of the discrepant results reported in the literature, while Section 5 discusses the implications for theoretical efforts. For a reader interested in a quick overview of the results and their implications, we suggest reading Section 6 first, followed by figure captions and Section 4. Throughout the work, we assume standard cosmology ($H_0 = 70$ km s^{-1} Mpc^{-1}, $\Omega_m = 0.3$, $\Omega_\Lambda = 0.7$).

2. DATA, SAMPLES AND MEASUREMENTS

SDSS spectroscopic survey (Strauss et al. 2002) represents the largest survey of galaxies in the local universe ($z < 0.2$) and has served as a primary source of data for studies that have described the MZR (T04) and the M_*–Z–SFR relation (M10, LL10). Thus, in this paper we also use SDSS as the basis for our work.

2.1. Sample Cuts

In this section, we describe the cuts we use to define the samples drawn from SDSS spectroscopic survey, and illustrate their effect on the properties of the sample in Figure 1. Definition of the sample in this paper follows the procedures adopted by M10 to select the star-forming galaxies. As in M10, we start with the MPA/JHU reduction of SDSS DR7 spectroscopic sample. MPA/JHU catalog[11] contains spectroscopic line measurements derived using a custom pipeline that yields continuum subtracted fluxes (T04). Full MPA/JHU SDSS DR7 sample consists of 928,000 galaxies (all sample numbers are rounded to the nearest thousand), but this number drops to 212,000 after the application of the M10 redshift ($0.07 < z < 0.30$) and Hα signal-to-noise ratio cuts (S/N(Hα) > 25). Relatively high signal-to-noise cut on Hα flux was applied in order to yield usable signal in other, weaker, emission lines that are necessary for the measurement of metallicities, while the relatively high low-redshift limit was chosen to ensure that spectroscopic fibers cover large fraction of each galaxy (2 kpc at $z = 0.07$ and 7 kpc at $z = 0.30$). Line flux errors are taken as listed in the MPA/JHU catalog.

[11] http://www.mpa-garching.mpg.de/SDSS/DR7

Next we follow M10 and apply minor cuts to remove anomalously low ($F(\mathrm{H}\alpha)/\mathrm{F}(\mathrm{H}\beta) < 2.5$) and very high Balmer decrements, i.e., dust attenuations ($A_V > 2.5$), bringing the sample to 203,000. The purpose of these cuts is to eliminate unphysical or extreme dust attenuation corrections. We presume that M10 follow Nagao et al. (2006), who determine the attenuation at V band from the Balmer decrement using Cardelli et al. (1989) extinction law:

$$A_V = 7.23 \log \frac{F(\mathrm{H}\alpha)/\mathrm{F}(\mathrm{H}\beta)}{2.86},$$

with the attenuation affecting the Hα line being related to A_V by

$$A_{\mathrm{H}\alpha} = 0.818 A_V.$$

Note that A_V is evaluated in the V band as a matter of convention, but it represents extinction in H II regions, which is typically several times larger than the extinction of the stellar continuum (Calzetti et al. 2000; Charlot & Fall 2000). Galaxies where emission line flux is dominated by non-stellar emission are removed using the Kauffmann et al. (2003) criterion on the BPT diagram (Baldwin et al. 1981) line ratios, coupled with the log N2 < -0.2 cut (N2 $= F([\mathrm{N\,II}]6584)/F(\mathrm{H}\alpha)$), leaving 160,000 galaxies.

In Figure 1, we show the effect of the cuts as reflected in the specific SFR versus stellar mass plane. Specific SFRs are derived from the UV–optical spectral energy distribution (SED) fitting and masses are taken from MPA/JHU catalog.[12] Figure 1(A) shows the initial sample. We see the well-known bimodality in star-formation properties, with mostly quiescent galaxies lying below log (SFR/M_*) $= -11.5$ and actively star-forming galaxies lying on a relatively narrow sequence (the "star-forming sequence" or the "main sequence"). The upper dotted line (repeated in all panels) represents the star-forming sequence fit from Salim et al. (2007, hereafter S07), and pertains to galaxies selected as star-forming according to Brinchmann et al. (2004, hereafter B04) criteria, and the lower line shows the SF sequence as determined in Salim & Lee (2012) using the Gaussian decomposition of the full sample into star-forming and passive galaxies. Application of the redshift cut (Figure 1(B)), applied following M10, removes the low-mass tail, especially among galaxies with less intense SF. As a result, for log $M_* < 10$, the sample tends to retain galaxies above the mean SF sequence relation. Application of the remaining M10 selection criteria, most importantly the Hα S/N cut and the BPT selection, removes quiescent galaxies but also eliminates a significant fraction of galaxies on the SF sequence (Figure 1(C)).

In consideration of the potential biases described above, we have also constructed an *augmented* sample, which retains all the cuts as the M10 sample except that it allows redshifts extending down to 0.005 as long as the fiber contains at least 10% (following Yates et al. 2012) of the total stellar mass (fiber masses are available from the MPA/JHU catalog). Even at lowest redshift, the majority of galaxies pass the fiber mass fraction criterion, so we do not expect a bias due to incompleteness. Note that SDSS mass covering fraction is typically 30% (95% of galaxies have the covering fraction between 17% and 50%). The augmented sample facilitates fuller characterization of the trends at log $M_* < 10$ (plot not shown). The augmented sample contains 259,000 galaxies (a 60% increase).

[12] Full description of various types of measurements is given in Section 2.3. The choice of SFR indicator in Figure 1 is of little importance.

2.2. Metallicities

In this work, we will use four metallicity indicators: (1) M10 metallicities—an average of R23 and N2 estimates, (2) Bayesian metallicities of T04, (3) N2O2, and (4) R23 with an O32 term. We will primarily use metallicity estimates determined following a procedure described in M10. We refer to these metallicities as M10 metallicities. M10 metallicities are the average of 12+log(O/H) estimates from two strong-line methods: R23 (the ratio of four oxygen lines ([O II]3727 doublet and [O III]4958, 5007) to Hβ, Pagel et al. 1979) and N2 (the ratio of [N II]6584 to Hα, van Zee et al. 1997). R23 and N2 metallicities were derived using relations from Maiolino et al. (2008), which calibrate various line ratios with respect to Kewley & Dopita (2002) theoretical metallicities of SDSS galaxies. All emission lines were corrected for dust attenuation using Hα-to-Hβ Balmer decrement and Cardelli et al. (1989) extinction curve. Following M10, we allow galaxies with log R23 < 0.9 and log N2 < -0.35 (the range of validity of Maiolino et al. 2008 calibrations) and remove those where the two metallicity estimates based on R23 and N2 differ by more than 0.25 dex. We confirm that neither of these cuts removes galaxies of any particular SFR range. The final M10-like sample (i.e., sample with M10 redshift cuts) consists of 141,000 galaxies (matching the number quoted in M10), while the final augmented sample (sample allowing $z < 0.07$) consists of 222,000 galaxies. The median redshift of the final M10-like sample is 0.11 and that of the final augmented sample is 0.08.

For comparison with previous work and to discuss potential biases affecting M10 metallicities, we will consider additional metallicity estimates. One is the metallicity estimate taken from the MPA/JHU catalog, which was derived following the methodology described in T04. T04 metallicities are different from most other estimates because they are not based on some line ratio calibrated against another metallicity estimate, but come directly from fitting the stellar-continuum subtracted spectra to emission-line photoionization model spectra containing multiple emission lines (four Balmer lines and eight forbidden lines). T04 metallicities are not publicly available for all galaxies for which we calculate M10 metallicities because the MPA/JHU catalog provides them only for galaxies classified as star-forming by B04 criteria. Those criteria required a S/N threshold of 3 in all four BPT lines, but with flux errors scaled up to account for the scatter in fluxes of repeat observations, thus effectively becoming equivalent to S/N ratio cuts of between 5 and 7. As a result, of 141,000 (222,000) galaxies in the final M10-like (augmented) sample 93,000 (163,000) have T04 metallicities (∼60%).

Recently, Juneau et al. (2014) revisited the analysis of repeat observations and showed that flux error scalings are much smaller for *flux ratios* (needed for BPT classification and metallicity determinations) than for absolute fluxes and are very close to one. Therefore, in this paper, we do not scale flux errors.

We will also derive metallicities using the N2O2 method (the ratio of [N II]6584 to [O II]3727) for which theoretical calibration is taken from Equation (7) in Kewley & Dopita (2002) and using the R23+O32 method (R23 method with an O32 ([O III]4958, 5007 to [O II]3727 line ratio) term McGaugh 1991), based on theoretical calibration from Equation 18 in Kobulnicky & Kewley (2004). Unlike the M10 metallicities, these two methods are expected either to be less dependent on the ionization parameter (N2O2) or to explicitly correct for it (R23+O32).

2.3. Star Formation Rates and Stellar Masses

In this study, we will primarily use four measurements of SFR. Two pertain to SFR contained within the SDSS spectroscopic fiber, and two are integrated (total) SFRs. Following M10, we calculate fiber SFR from the Hα luminosity, dust corrected with a Balmer decrement and converted to SFR using Kennicutt (1998) conversion. Another fiber SFR estimate comes from the MPA/JHU catalog, determined according to B04 method of fitting photoionization models to six emission lines (including Hα and Hβ) simultaneously. As in the case of T04 metallicities, the method does not apply any explicit conversions to obtain the target parameter (metallicity or SFR), but performs Bayesian fitting of fluxes or flux ratios. B04 have shown that photoionization models imply that the conversion between the dust-corrected Hα and SFR is strongly metallicity (and therefore, indirectly, mass) dependent. As a result, B04 SFRs can be as much as 0.5 dex higher for the most metal-rich galaxies. Fiber SFRs, originating from nebular emission of very massive stars, measure instantaneous SFR (timescale <10 Myr).

First of the two total SFRs comes from the SED fitting of *GALEX* (Martin et al. 2005) ultraviolet (UV) and SDSS optical broadband photometry. We perform SED fitting on all SDSS spectroscopic sample galaxies covered by *GALEX* medium-deep imaging (50% of SDSS area). Fitting includes galaxies covered but not detected by *GALEX*, invariably non-SF galaxies, thus keeping the sample optically selected. SED fitting is performed using Bayesian approach by comparing the observed fluxes with a library of model fluxes obtained from stellar population synthesis models (Bruzual & Charlot 2003) using some priors on star-formation history and attenuated according to the Charlot & Fall (2000) dust extinction model. The methodology is described in detail in S07. Principal differences with respect to S07 are that we now use model priors optimized for star-forming galaxies (as described in da Cunha et al. 2008) and we produce model libraries more finely sampled in redshift (0.01 versus 0.05 in S07). SED SFRs, being mainly constrained by UV, are determined as averaged over the past 100 Myr.

Second type of total SFRs come from 22 μm ($W4$ channel) observations from *WISE* (Wright et al. 2010). We use the AllWISE catalog profile-fit $W4$ fluxes[13] and extrapolate them using Dale & Helou (2002) IR SEDs calibrated with Marcillac et al. (2006) relations to obtain the total IR luminosity, which is then converted to SFR using the Kennicutt (1998) relation. Details can be found in Salim et al. (2009), where the same procedures were used on *Spitzer* 24 μm fluxes. Detections at 22 μm are available for 54% of the final sample, but this incompleteness does not produce strong biases in SSFR–M_* parameter space (Figure 1(D)). Mid-IR emission is typically assumed to originate from dust-enshrouded young populations that also give rise to the UV emission and therefore are expected to trace current ($\sim$100 Myr) SFR. However, Salim et al. (2009) have shown that mid-IR may have significant contributions from older populations even in actively star-forming galaxies, so that the timescale over which mid-IR measures SF may be effectively on the order of few gigayears.

We will also be considering specific SFRs. Fiber SSFRs are obtained by normalizing fiber SFRs by fiber stellar masses from the JHU/MPA catalog. SED SSFRs are derived directly from the SED fitting and mid-IR SSFRs are normalized by the total stellar mass from the JHU/MPA catalog. As in M10, we use stellar masses from the JHU/MPA catalog, which were derived from SDSS photometry (following but independent from S07). These masses are in a very good agreement (scatter in difference $\sim$0.08 dex, with $<$0.01 dex overall offset) with the masses obtained from our SED fitting.

For all MPA/JHU measurements (metallicity, SFRs, stellar masses) and for parameters from the SED fitting, we use medians of the probability distribution function as fiducial parameter values.

SFRs and stellar masses were either derived with or converted to Chabrier IMF.

3. M_*–Z–SFR RELATION IN THE LOCAL UNIVERSE: EMPIRICAL ANALYSIS FRAMEWORK AND SYSTEMATICS

3.1. Setting the Stage: Identifying the Physically Motivated Secondary Parameter in the M_*–Z Relation

In this section, we set the stage for the remainder of our analysis by identifying the optimal and the most physically motivated parameter driving the secondary dependencies in the MZR. We then use this knowledge to propose an intuitive framework for investigating the M_*–Z–SFR relation in Section 3.3.

A useful way to think of the M_*–Z–SFR relation is that it is represents an extension of a familiar MZR. Thus, a commonly used way to illustrate the SFR dependence is to show average (or median) mass–metallicity tracks of galaxies selected to lie in different bins of *absolute* SFR (e.g., M10, Yates et al. 2012; Andrews & Martini 2013; Nakajima & Ouchi 2014). In this section, we will show that the absolute SFR is not the optimal quantity with which to characterize MZR residuals. The choice to use absolute SFR as a secondary parameter in the mass–metallicity relationship is probably motivated by the fact that the M_*–Z–SFR relation has originally been formulated by M10 and LL10 as the relation between the mass, metallicity, and SFR. Instead, we argue that this should rather be the *relative* SSFR—the difference between galaxy's SSFR and the SSFR typical for galaxies of that mass (i.e., the offset from the star-forming sequence).

To show this, we will contrast MZRs (Figure 2) of samples selected to have the extreme (highest 2.5% (top panels)) and the lowest 2.5% (lower panels)) values of (1) absolute SFR (left panels), (2) absolute SSFR (middle panel), and (3) relative SSFR (right panels) to the MZR of the general population of galaxies (repeated green band in each panel is the 90 percentile range of the metallicities of the overall M10-like sample). Median trends of top (bottom) samples is shown as a purple (red) line, and of the general population as a white line. In Section 3.1, we will only be using M10 metallicities and SFRs derived in SDSS spectroscopic fibers, as derived in M10. Thus our Figure 2 is directly comparable to Figure 1 in M10.

We begin this exercise by exploring MZR offsets due to absolute SFRs. We see that the galaxies with the highest SFRs (Figure 2(A)) show no offset with respect to the overall sample at the highest masses ($\log M_* > 11$), while at $\log M_* = 10$ the offsets have increased to 0.2 dex, and stay that large at lower masses. Since SFRs on average increase with mass (e.g., B04), the highest SFRs are preferentially found among the more massive galaxies. Likewise, the galaxies with the lowest SFRs will be found in the region of lower masses (panel (B)). Galaxies with the lowest SFRs are systematically offset *above*

[13] We confirmed that mid-IR SFRs from the profile-fit photometry produce smaller scatter with respect to other SFRs than the standard aperture *WISE* photometry.

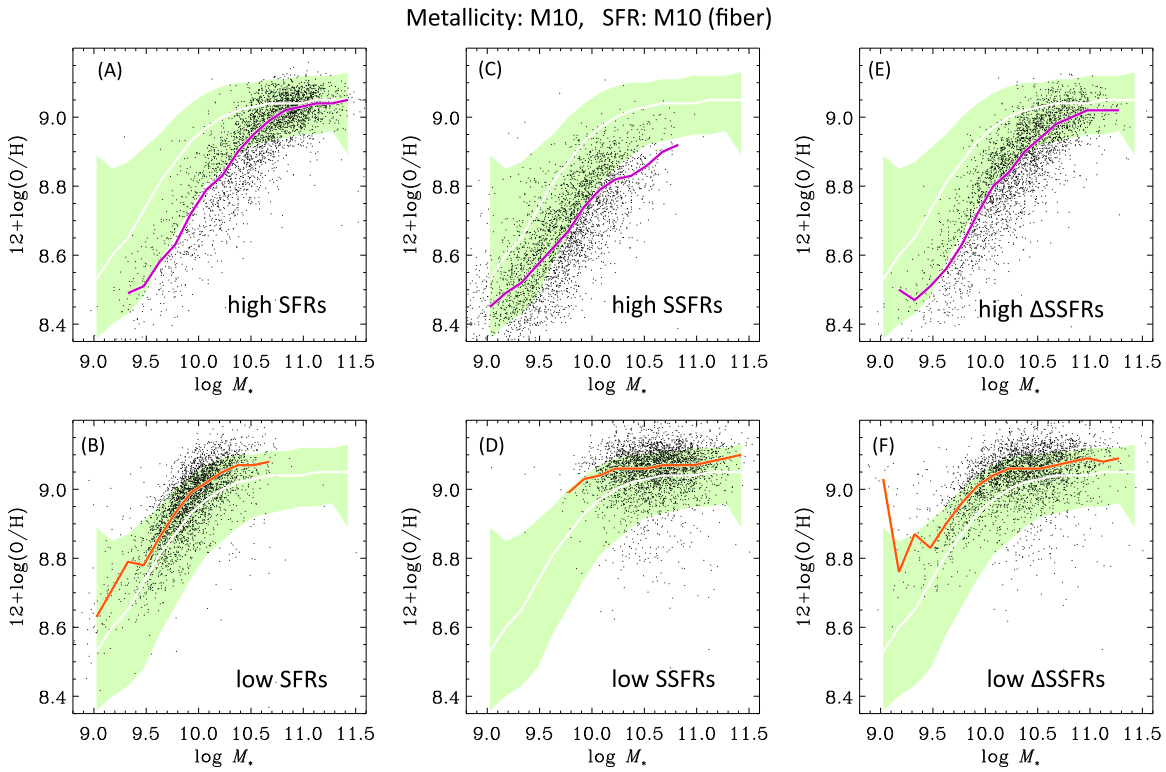

Figure 2. Mass–metallicity diagrams of galaxies selected to be extreme according to some SFR-related parameter. The upper (lower) row of panels show galaxies with the highest (lowest) 2.5% of values in the sample (for E and F, extreme in each mass bin). Sample selection follows M10 (our "M10-like" sample), which features an Hα S/N cut of 25, but no S/N cuts on other emission lines. Panels (A) and (B) select by SFR, (C) and (D) by specific SFR, and (E) and (F) by specific SFR in a given mass bin. Fiber-based measurements are used in all panels. In all panels, green shaded regions give the 90 percentile range of the overall M10-like sample, with the white line representing the median. All mass bins are 0.15 dex wide. Medians of the high/low samples (colored lines) are showed when more than five galaxies exist in a bin.

(A color version of this figure is available in the online journal.)

the median overall MZR, by some 0.05 dex, regardless of the mass.

Given that the SFR to first order simply scales with mass, it is justified, and physically more motivated (e.g., Ellison et al. 2008; Yates et al. 2012), to explore whether the SFR normalized by mass, i.e., the specific SFR—an indication of the current SF activity with respect to the past average—would produce stronger offsets across the mass range than just the SFR. We again show M_*–Z plots, but now for 2.5% of the sample with highest and lowest SSFRs in the sample (Figures 2(C) and (D)). Since on average, the specific SFR declines with increasing mass (e.g., S07, also Figure 1), we now have the reverse situation that the highest SSFRs are found among the lower-mass galaxies and the lowest SSFRs are among the more massive. Median offsets for the intense star-formers remain large at high masses, but they are somewhat smaller than in the case of top SFRs for the lowest masses. For galaxies with low SSFRs (panel (D)), there is not much overlap in the mass regime with low SFRs (panel (B)), and the median MZR also sits some 0.05 dex above the overall median.

One can see that considering galaxies selected by either SFRs or SSFRs implicitly introduces a mass selection. A true secondary parameter driving offsets in MZR should apply to galaxies of all masses. Thus we now explore samples selected by the level of SSFR *relative* to what is typical at a given mass. Relative SSFR ($\Delta \log \mathrm{SSFR}$) is defined as

$$\Delta \log \mathrm{SSFR} = \log \mathrm{SSFR} - \langle \log \mathrm{SSFR} \rangle_{M_*},$$

where $\langle \log \mathrm{SSFR} \rangle_{M_*}$ is the median or mean of $\log \mathrm{SSFR}$ of galaxies having a mass M_*. In this work we use medians in 0.15 dex wide mass bins. Relative SSFR can be visualized as the offset of a galaxy from the star-forming sequence (vertical distance in Figure 1), a measure also called "SFR excess" (Schiminovich et al. 2007) or "starburstiness" (Elbaz et al. 2011). The relative SSFR is a "natural" parameter to characterize star-formation activity and is becoming increasingly used in the recent literature (e.g., Magdis et al. 2012; Woo et al. 2013). In Figures 2(E) and (F), we now show galaxies with the highest and lowest 2.5% relative SSFRs in each mass bin. These galaxies typically have SSFRS that are five times higher/lower than typical values at that mass ($|\Delta \log \mathrm{SSFR}| > 0.7$ dex). The quantity of points at different masses now reflects the mass distribution in the overall sample. We notice that some offset for highly star-forming galaxies (panel (E)) is now present even at the highest masses, which was not the case when absolute SFRs were considered (panel (A)). At lower masses, the offsets are at least as strong as they were in panel (A), but now the selection includes more galaxies. Similarly, for galaxies with the lowest relative SSFRs (panel (F)), the offsets are as large as in the case of either the lowest SFRs or SSFRs, but spanning the full range of masses.

From this section, we conclude that MZR offsets are more naturally characterized by the difference between the logarithm of galaxy's SSFR with respect to a typical log SSFR at a given mass, rather than the absolute SFRs. In hindsight, this may seem fairly obvious, but this point has not has not previously been clearly made. The interpretation of the MZR offsets in terms of the variations of relative SSFR is more in accordance with FMR's evolutionary sense: at higher redshifts the SF sequence appears to shift upward without much change in the slope (e.g.,

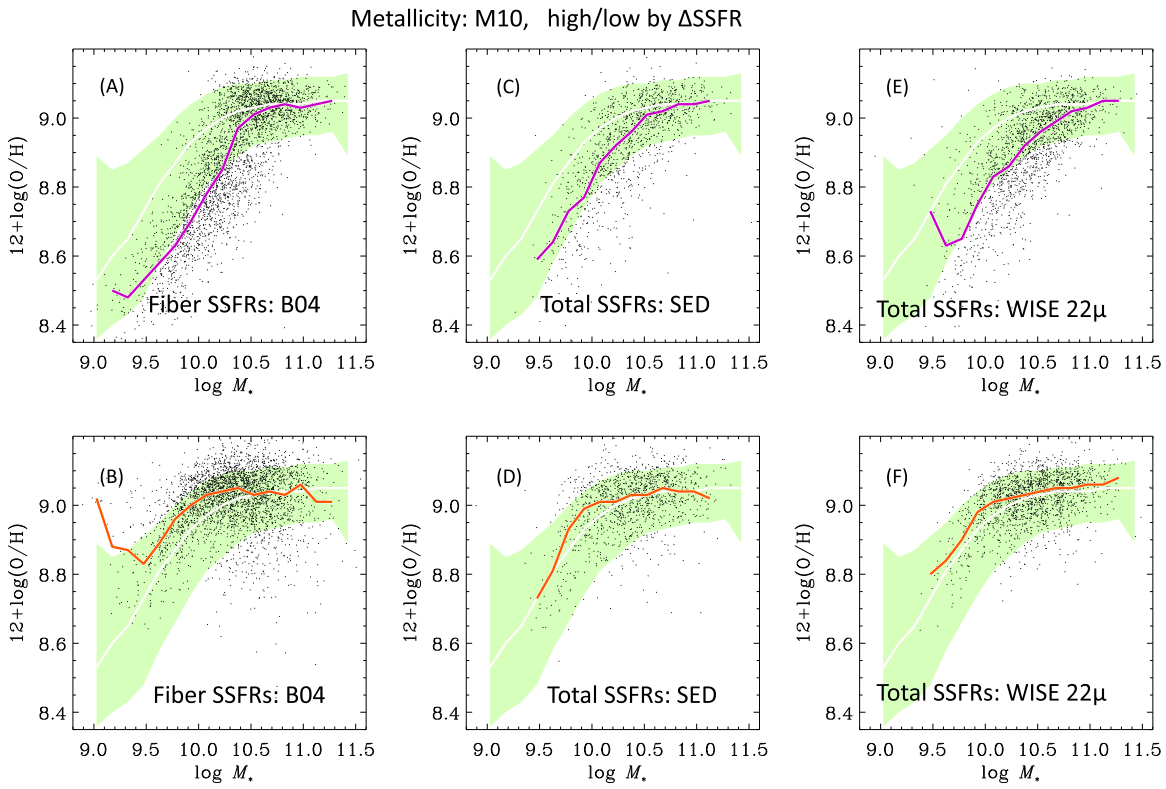

Figure 3. Mass–metallicity diagrams of galaxies selected to have extreme SSFRs at fixed mass, where the SFR has been calculated using different indicators. As in the previous figure, the upper (lower) row of panels show galaxies with the highest (lowest) 2.5% of values in the sample, and the green region shows the 90 percentile range of the overall "M10-like" sample. Panels (A) and (B) show samples selected by Brinchmann et al. (2004) fiber SSFR, (C) and (D) by total SSFR derived from broad-band UV/optical SED fitting, and (E) and (F) by total SSFR derived from 22 μm mid-IR luminosity (*WISE* channel *W*4).

(A color version of this figure is available in the online journal.)

Speagle et al. 2014), so considering local samples at some distance (offset) from the SF sequence is more analogous to a high-redshift selection.

Does the above mean that the functional form of $Z(M_*$, SFR) should feature SSFR rather than SFR? In the case of a linear relationship and *total* measurements, the two formulations are formally equivalent. However, for *fiber* measurements, the difference is crucial. Fiber SFR, used in M10's formulation of FMR (their Equations (2), (4), and (5)), is not a meaningful physical quantity since it depends, to the zeroth order, on galaxy distance: on average, SDSS fibers cover 25% of SF at $z = 0.07$, but 65% at $z = 0.30$. On the other hand, fiber *specific* SFR (fiber SFR normalized by mass in the fiber) is a perfectly valid physical quantity, representing the intensity of SF in the *same physical region* of the galaxy in which the metallicity is measured and is therefore probably even preferred to the total specific SFR for the purposes of M_*–Z–SFR analysis. Future studies should report their fiber or slit SSFRs to allow for a more direct comparison with SDSS. Surprisingly, M10 find that their least-scatter projection, formulated with *fiber SFRs*, agrees with high-redshift measurements, even though fiber SFRs are distance-dependent and are on average 0.6 dex smaller than the total SFRs (but with a substantial, distance-dependent scatter). Altogether, it makes more sense to formally describe M_*–Z–SFR relations using specific SFRs. Indeed, the recent analytical model of Lilly et al. (2013, e.g., their Equation (40)) finds the metallicity to be the function the SSFR (see discussion in Section 5).

Guided by the inferences made in this section, in the rest of the paper we will consider the relative SSFR as the primary independent variable for galaxies of a fixed mass.

3.2. How Dependent is M_*–Z–SFR Relation with Respect to the Type of SFR Indicator?

Previous work onM_*–Z–SFR relation in SDSS used exclusively SFRs derived based on the emission lines measured in spectroscopic fibers. As some of those same line measurements are involved in the determination of metallicity, this opens a concern that the M_*–Z–SFR relation may to some extent be the result of spurious correlations between the measurements of SFR and the metallicity. Therefore, in this paper, we will examine the relationship with two completely independent total SFRs, based on integrated fluxes. Furthermore, different SFR indicators are sensitive to SF over different timescales, which in principle may be more or less strongly tied to the changes in the metallicity.

In this section, we investigate four SFR indicators: two measured in fibers (both based on emission lines, but one following M10's common methodology of Balmer decrement-corrected Hα luminosity, and the other using B04's more sophisticated methodology of modeling simultaneously multiple emission lines) and two total measurements (one based on the UV/optical SED fitting, and the other based on 22 μm mid-IR luminosity from *WISE*). The results are presented in Figure 2 (right panels—M10 SFRs), and are continued in Figure 3 (left panels—B04 SFRs; middle panels—SED SFRs; right panels—mid-IR SFRs). In Figure 3, we continue to plot the galaxies with 2.5% highest/lowest *relative* SSFRs (top/bottom panels), and contrast them to the general population of galaxies (green band). We continue to use M10 metallicities.

We begin with the comparison of M_*–Z plots based on M10 fiber SFRs (Figures 2(E) and (F)) to B04 fiber SFR (Figures 3(A)

and (B)). Below $\log M_* = 10.3$ there is not much difference in MZRs of either the high or the low SSFR samples selected by either M10 or B04 SSFRs. Above $\log M_* = 10.5$, galaxies selected by B04 SSFR show no offset with respect to the overall metallicity. Since B04 SFRs are more sophisticated than M10 SFRs and therefore presumably more accurate, this suggests that there is very little or no SFR dependence in the MZR above $\log M_* = 10.5$.

Next we look at SED SFRs—total SFRs determined from the UV/optical broadband fluxes, and primarily constrained by the UV. The MZR of the most intensely star-forming galaxies (Figure 3(C)) shows approximately two times smaller offset below $\log M_* = 10.3$ with respect to equivalent relations based on either fiber SFRs. Above, $\log M_* = 10.5$, the offset is nearly gone, as in the case of B04 fiber SFRs. For galaxies selected to have the lowest relative SSFRs (Figure 3(D)), the offset is likewise smaller than for fiber SFRs and basically not present above $\log M_* = 10.3$, again similar to B04 SFRs. Before drawing any conclusions, we examine high/low samples selected by mid-IR SFRs. For intense star-formers (Figure 3(E)), the offset in MZR is, surprisingly, again as strong as it was for M10 fiber SFRs and is clearly present even at $\log M_* = 10.5$, which was not the case for either B04 fiber SFRs or for the total SED SFRs. For galaxies furthest below the SF sequence (but detected at 22 μm), the offset is quite small (0.02 dex), as in the case of SED SFRs, and unlike M10 SFRs. We have verified that this small offset is not because of 22 μm detection limit potentially eliminating lowest star-formers—if we produce M10 SFR selected M_*–Z plot (not shown) but only for galaxies also detected at 22 μm, we still obtain an offset as large as the one in Figure 2(F).

To conclude, we find that the dependence of MZR on SSFR is definitely present using all SFR indicators, whether they be fiber or total, so the M_*–Z–SFR relation cannot be merely an artifact of correlated measurements. The degree of offsets vary, but at least one SSFR of both types (fiber and total) shows equally strong offsets for highly SF galaxies. It is interesting that the dependence is not significantly weakened when using total SSFRs, considering that the metallicity is measured in the fiber. Note that if an SSFR measure has a high uncertainty, it will not be able to accurately identify galaxies that are truly the highest star-formers and therefore the most discrepant in metallicity, which may explain why the trends are weaker using SED SFRs. This emphasizes the need to perform comparison of samples at different redshifts using indicators of similar accuracy, and, preferably, of the same type. Results further suggest that the fact that different indicators trace SF over different timescales does not appear to affect the trends significantly. Finally, we confirm previous findings (Ellison et al. 2008, M10) that the MZR offsets are more pronounced at lower masses, and that they are close to zero when approaching $\log M_* = 11$.

3.3. Characterization of the M_*–Z–SFR Relation

In previous sections, we used familiar M_*–Z plots and contrasted samples of galaxies selected to be extremes in terms of star-forming properties. We now wish to include all of galaxies in the analysis. We have also seen that the MZR offsets are strongly mass dependent. We therefore need to analyze galaxies of different mass ranges separately. Following the framework set up in Section 3.1, we do so by plotting the metallicities against the relative SSFR. These Z–ΔSSFR plots for galaxies belonging to some mass bin embody our non-parametric methodology for exploring the M_*–Z–SFR relation.

In Figure 4, we show four Z–ΔSSFR plots, for one of 0.5 dex wide mass bins centered on $\log M_* = 9.5$, 10.0, 10.5, and 11.0. Results do not depend strongly on the width of mass bins. We continue to use M10 metallicities and revert to M10 fiber SSFRs, but from now on use the *augmented* sample (one extending to lower redshift, $z = 0.005$, than what was used in M10), which allows for better characterization of the low-mass regime (Section 2.1). Relative SSFR for a given galaxy is determined as the difference of its SSFR with respect to the median SSFR in 0.15 dex wide mass bin. Positive relative SSFRs correspond to galaxies sitting above the star-forming sequence. Almost identical results would be obtained if, instead of using running medians, the relative SSFR was calculated as the difference between SSFR and the SSFR corresponding to the linear fit of log SSFR versus $\log M_*$ at that mass (such as those in Figure 1). Figure 4 now allows us to explore dependence of Z on SSFR for all galaxies, not just those at the extreme of SSFR distribution.

We start from the mass bin centered on $\log M_* = 9.5$ (Figure 4(A)), where the metallicity trend is stronger than in higher mass bins. Fitting the linear relationship (purple line) yields a slope $\kappa = d(12+\log(\mathrm{O/H}))/d\log(\mathrm{SFR}/M_*)$ of -0.18. However, running medians reveal that the SFR dependence is considerably stronger above the SF sequence (a linear fit would yield, $\kappa_{\rm high} = -0.26$), then in its core and below it ($\kappa_{\rm low} = -0.12$). Moving on to the next mass bin (Figure 4(B)), we find that the overall dependence on SFR gets weaker ($\kappa = -0.12$), but again the slope is steeper above the SF sequence than in its core and below it. Remarkably, the slope above the SF sequence is as steep as in the lower mass bin (values of slopes are given in Table 1). At $\log M_* = 10.5$ (Figure 4(C)), the overall slope is only $\kappa = -0.05$, and while it is again steeper above the SF sequence (and still as steep as at lower masses), the steepening does not begin until 0.7 dex above the sequence and consequently encompasses only a small number of highly star-forming galaxies. Finally, in $\log M_* = 11.0$ bin (Figure 4(D)), we stop seeing different behavior above and within/below the SF sequence, with a rather shallow overall trend of $\kappa = -0.03$.

Are the results presented here valid for total SSFRs? We list the slopes of metallicities against the offset from the SF sequence based on mid-IR SFRs in Table 1). The results are remarkably similar to those based on fiber SFRs, with the most notable difference being that the slope in the highest mass bin is even weaker. This basically confirms the conclusion from Section 3.2 that the differences in timescales of SFR indicators and whether they pertain to fiber or integrated measurements do not lead to great differences in metallicity's dependence on SSFR.

To conclude, in this section, we have demonstrated that the metallicity's dependence on SSFR is stronger *above* the SF sequence (as remarked by M10). And while the dependence for the bulk of galaxies (those in and below the SF sequence) weakens as the mass goes up, the dependence for intense star-formers (lying at $\gtrsim$0.6 dex from the SF sequence) stays very similar, suggesting that the different mechanisms drive the M_*–Z–SFR relation depending on SF intensity, which itself may be related to the existence of different modes of SF (e.g., quiescent versus merger-driven). Some studies, especially at $z \gtrsim 1$, distinguish populations with high relative SSFR (e.g., Δ log SSFR > 0.3, Elbaz et al. 2011) as having a special mode of star formation associated with mergers and label them "starbursts." However, at $z \sim 2$, the starbursts produce a clear excess above the Gaussian distribution of log SSFR and dominate already at $\Delta \log \mathrm{SSFR} = 0.6$ (Rodighiero et al. 2011).

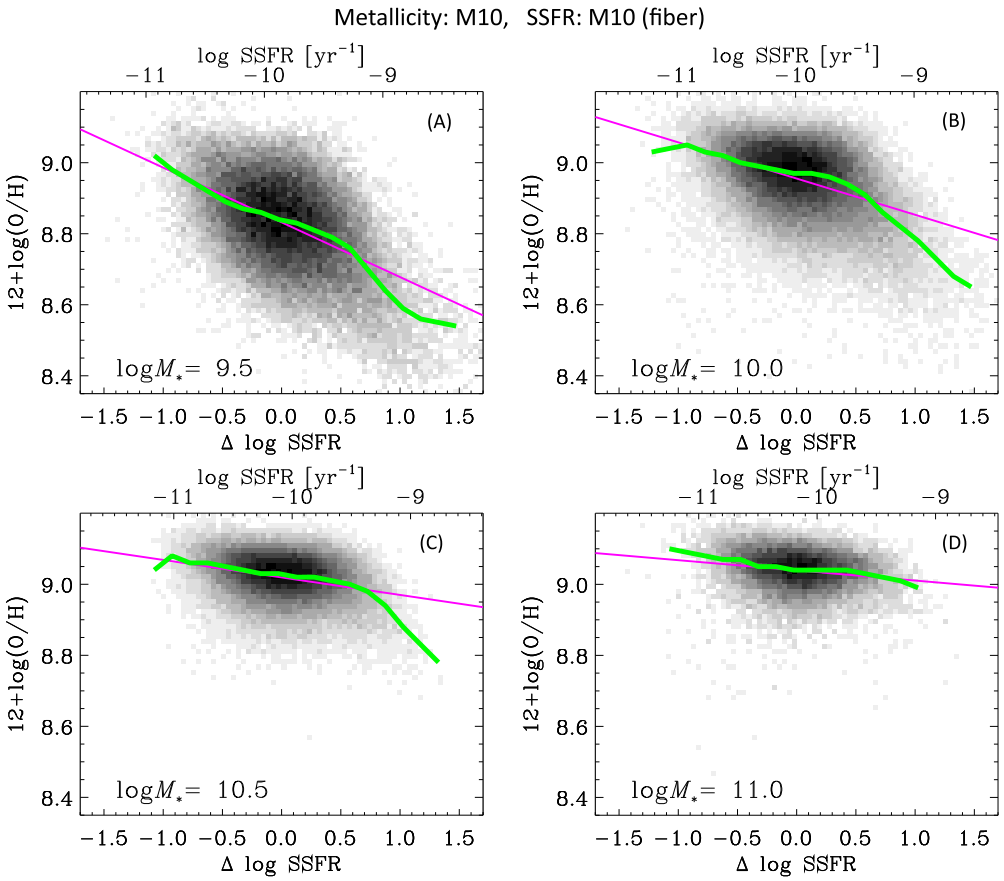

Figure 4. Dependence of the metallicity on the offset from the star-forming sequence, in different mass bins. Both the metallicity and the fiber SFRs are as derived in M10. We now use an augmented sample, which follows the M10 selection (most importantly the Hα S/N cut of 25) but allows redshifts down to 0.005 as long as the mass contained in fiber is at least 10% of the total galaxy mass. Mass bins are centered on the values indicated in each panel, and are 0.5 dex wide. The absolute SSFR at the center of the mass bin is given along the top of each plot. Magenta lines show linear fits to the data points, while the green lines represent medians (when at least 15 galaxies exist in a 0.15 dex wide bin). Grayscale uses square-root scaling in order to better display the full dynamic range of the density of data points. A SSFR dependence is present at all masses, but is stronger at lower masses. It also depends on the SSFR itself, and is stronger above the star-forming sequence in the three lower mass bins.

(A color version of this figure is available in the online journal.)

Table 1
Characterization of the M_*–Z–SFR Relation

SFR type	log M_*	Median 12+log(O/H)	σ(12+log(O/H))	$\sigma_{\rm corr}$(12+log(O/H))	κ	$\kappa_{\rm low}$	$\kappa_{\rm high}$	Break point
M10 (fiber)	9.5	8.83	0.121	0.102	−0.15	−0.12	−0.27	0.6
M10 (fiber)	10.0	8.96	0.092	0.081	−0.10	−0.06	−0.29	0.5
M10 (fiber)	10.5	9.02	0.063	0.059	−0.05	−0.04	−0.32	0.7
M10 (fiber)	11.0	9.03	0.052	0.051	−0.03	−0.03	−0.16	0.7
WISE 22 μm (total)	9.5	8.85	0.119	0.107	−0.17	−0.14	−0.16	0.3
WISE 22 μm (total)	10.0	8.96	0.089	0.082	−0.11	−0.08	−0.19	0.5
WISE 22 μm (total)	10.5	9.02	0.060	0.058	−0.04	−0.03	−0.21	0.6
WISE 22 μm (total)	11.0	9.04	0.049	0.049	−0.01	−0.01	−0.22	0.7

Notes. Median 12+log(O/H) is given at the position of the SF sequence according to the linear fit. Scatter in metallicities around the running median, i.e., corrected for SFR dependence is $\sigma_{\rm corr}$(12+log(O/H)). Slope of the metallicity vs. the change in relative SSFR (i.e., the offset from the SF sequence) is κ, while the slopes above and below the break point (dex above the SF sequence) are $\kappa_{\rm high}$ and $\kappa_{\rm low}$. All metallicities are derived as in Mannucci et al. (2010, M10).

However, while we find the high-end distribution of log SSFR in SDSS to eventually depart from a Gaussian, this excess does not become dominant (twice as high as the Gaussian) until Δ log SSFR > 1.0 dex (for M10 SFRs, at log $M_* = 10$), well above the onset of break in the Z–SSFR relation. Therefore, we refrain from equating the two-mode behavior in metallicity trends with the normal SF versus merger-driven starburst distinction at this time, but do not rule out such a connection.

Important implication of this finding is that describing or extrapolating the SFR dependence using simple linear trends (equivalent to assuming a flat "fundamental plane" in LL10 or a single preferred projection of the FMR in M10) could lead to inconsistencies when comparing to high-redshift samples, as the local trends will be dominated by galaxies that show weaker SFR dependence. We see that using a single linear trend can produce discrepancies as large as 0.2 dex in the metallicity

for the most active star-formers. Such difference can give very different character to the interpretation of high-redshift data. Recently, Maier et al. (2014) showed (their Figure 5) that using different descriptions of the M_*–Z–SFR relation by M10 (second-order polynomial versus the plane of the least scatter) produce different extrapolations for high-SSFR samples. At a given mass, a better way to parameterize the SSFR dependence is with a broken linear fit—one for galaxies above the SF sequence and other for the rest. Ultimately, to test whether high-redshift samples follow the local M_*–Z–SFR relation (and to determine whether they exhibit the dependence on SSFR internally), it is best to show both the local and the high-redshift data on metallicity versus SSFR plots, within some mass bin (lower masses will provide stronger diagnostic as long as samples are not too small). We apply this methodology in S. Salim et al. (in preparation) to test whether local M_*–Z–SFR relation is consistent with $z \sim 2.3$ measurements.

3.4. Does Accounting for SFR Lead to a Considerable Decrease in the Scatter of the MZR?

The existence of the (S)SFR-dependence of MZR implies that if the (S)SFR was accounted for, the scatter in the relation would decrease. This decrease was presented in M10 as being dramatic. For example, their Figure 5 shows that the scatter in metallicity becomes a factor of almost three smaller (goes from 0.055 dex to 0.02 dex). However, what is perhaps not sufficiently appreciated is that this calculation in M10 pertained to the reduction of the rms residuals of *median-binned* values of metallicity around the best-fitting surface, and not of the individual galaxies. Different studies have claimed conflicting results regarding the scatter of individual galaxies (non-binned samples). Ellison et al. (2008) reported that SSFR is not an important cause of scatter in MZR (a 10% reduction) and more recently, Pérez-Montero et al. (2013) quoted a 0.01 dex reduction. These results are at odds with the M10 stated reduction from 0.08 dex to 0.05–0.06 dex.

The methodology applied in Section 3.3 allows us to directly address the question of the reduction of scatter. Figure 4 shows that the scatter in metallicity is high even at a fixed mass and fixed SSFR (metallicity axis in Figure 4 spans the exact same range as in $M_* - Z$ plots: Figures 2 and 3). Even at low masses ($\log M_* = 9.5$) where the SFR dependence is the strongest, the overall scatter (standard deviation) in metallicities of 0.12 dex is reduced only to 0.10 dex (scatter around the median), a 20% reduction. The effect is even more modest at higher masses, where the dependence on SFR is weaker. The values of the standard deviation of metallicities before and after accounting for the SFR are given in Table 1. The uncertainty in the measurement of SSFR ($\sim$0.2 dex) adds to the scatter in Z, but this contribution (0.2κ) does not account for more than 10% of the residual scatter. Based on this, we conclude that presenting the MZR using a quantity that combines the mass and SFR (as in M10 Figure 5) should not be expected to reveal conspicuous reduction in the scatter for typical samples of galaxies. On the contrary, the reduction is indeed very modest. This also means that the M_*–Z–SFR relation, as a three-dimensional "surface," is not particularly thin, despite common wisdom (e.g., Steidel et al. 2014), possibly inspired by M10's use of the *binned* points (e.g., their Figure 2).[14]

[14] To illustrate how binning can lead to a wrong impression, imagine a homogeneous spherical distribution of points in three-dimensional space xyz. Now perform binning of z values in bins defined in the xy plane. The binned values would form a perfectly thin *plane*.

Finally, we turn to another question regarding the scatter in Z. T04 and Zahid et al. (2012) have previously noted that the metallicity scatter in MZR, which becomes quite large at lower masses, is not due to, for example, larger measurement errors, but is intrinsic. The question is whether it can be fully explained by dependence on SFR. As we have seen, taking into account the SSFR dependence reduces the scatter at $\log M_* = 9.5$ from 0.12 only to 0.10 dex, which is still significantly larger than the typical metallicity errors at that mass (0.04 dex, T04). This suggests that some other parameter(s) may ultimately be more closely connected with metallicity regulation than the SFR.

3.5. Is M_*–Z–SFR Relation Sensitive to the Choice of Metallicity Measurements?

In this section, we explore how M_*–Z–SFR relation is affected by the use of alternative metallicity indicators, primarily those based on T04 method. Since T04 metallicities that are available in MPA/JHU catalog also involve additional selection criteria, we first need to explore if such criteria *alone* affect the dependence on SFR. In the analysis, we will continue to use Z–Δ SSFR plots split by mass bins.

Given all the practical and theoretical difficulties concerning the measurement of metallicities (e.g., Andrews & Martini 2013 and references therein), it is of critical importance to understand if different methods of deriving them affect the conclusions regarding the existence and the character of M_*–Z–SFR relation. In all of our analyses up to this point, we have used metallicities derived according to the method of M10, i.e., an average of estimates based on R23 and N2 calibrations of Maiolino et al. (2008). T04 metallicities, being available as part of the MPA/JHU catalog, are very often used in the analysis of SDSS samples and have been used for the characterization of M_*–Z–SFR relation (Lara-López et al. 2010; Yates et al. 2012). However, T04 metallicities are not available for the entire sample that we considered so far (which was selected by requiring S/N(Hα) > 25). Instead, T04 metallicities are available for galaxies satisfying the condition of having relatively high S/N ratios in all four BPT lines (S/N ratio >7.3, 5.5, 4.5, and 6.0 in Hα, Hβ, [O III]5007, and [N II]6584, respectively), as explained in Section 2.2, which is fulfilled for two-thirds of our sample. To see whether multiple S/N ratio cuts alone bias the trends, we repeat Figure 4, i.e., we still use M10 metallicities, but now restricted to those galaxies for which T04 metallicities exist. The resulting trends, in same mass bins as before, are shown in Figure 5. Comparison with Figure 4 reveals that while the overall trends are similar, there are important differences. Namely, the median metallicities *below* the SF sequence ($\Delta \log \mathrm{SSFR} < 0$) are now lower by up to 0.05 dex. There is no change above the SF sequence. In other words, the selection based on four emission lines leads to the preferential removal of galaxies with lower SSFRs and higher metallicities. The overall result is that the bulk trends (purple lines in Figure 5) become slightly weaker.

Keeping in mind the biases introduced by S/N ratio cuts present in T04 sample, we now look at the SSFR trends using the actual T04 metallicities (Figure 6). The results are remarkably different compared to equivalent plots made with M10 metallicities (Figure 5). In the lowest mass bin (panel (A)), where the dependence on SFR was the strongest, it is now much weaker, with the overall slope of only $\kappa = -0.05$. More importantly, the sense of the $Z(M_*, \mathrm{SFR})$ (that the more active galaxies at a given mass should have *smaller* metallicities) is only observed above the star-forming sequence ($\Delta \log \mathrm{SSFR} > 0.5$, and therefore involves a smaller fraction of galaxies. Bulk of

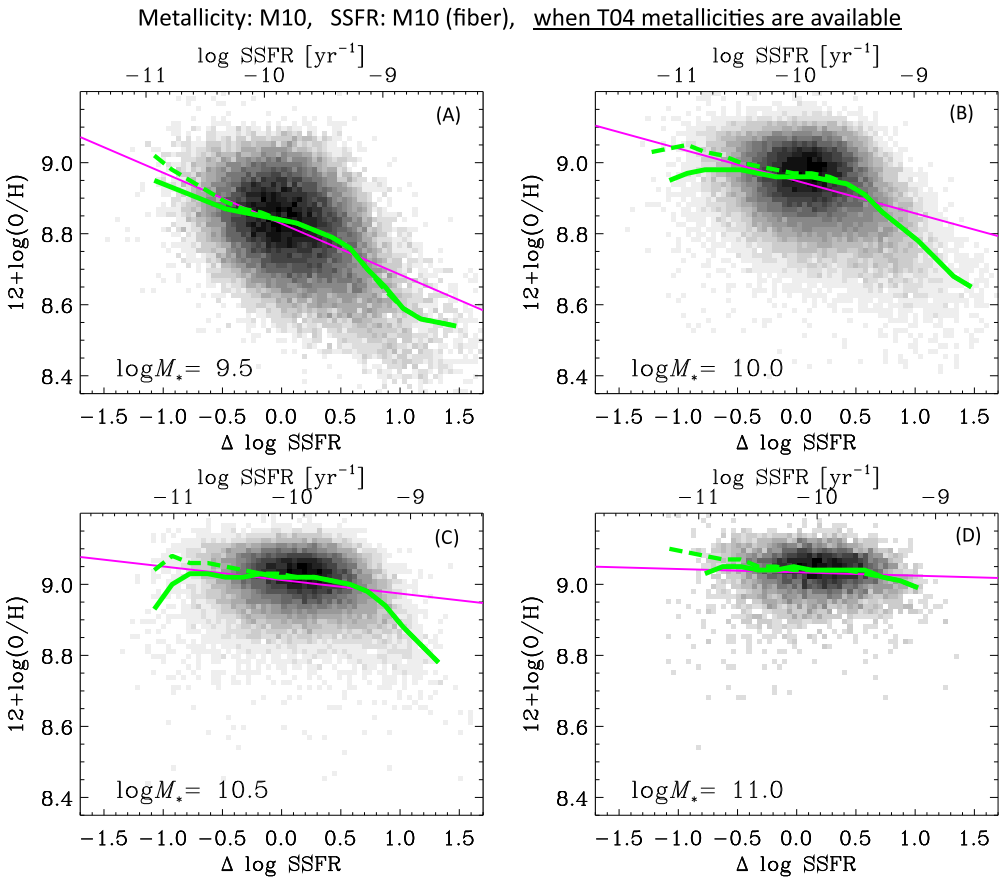

Figure 5. Dependence of metallicity on the offset from the star-forming sequence in different mass bins. This figure uses the same measurements as Figure 4, except that it shows only those galaxies from the augmented sample (∼two-thirds) for which Tremonti et al. (2004, T04) metallicities are available. Unlike the selection in the M10 sample, T04 metallicities require relatively high (>5–7) signal-to-noise ratio in all four BPT lines. Such multiple-line selection biases (weakens) the metallicity dependence on SSFR below the SF sequence (Δ log SSFR < 0) by preferentially eliminating galaxies with lower SSFRs and higher metallicities. Dashed lines show median metallicities prior to selection by T04 availability and demonstrate the effect of the S/N selection.

(A color version of this figure is available in the online journal.)

the galaxies (those within the core of the star-forming sequence and below it) show no trend at all. Similar situation persists in higher mass bins. Anti-correlation between metallicity and SFR is observed only at $\gtrsim$0.4 dex above the SF sequence, but for the bulk of the galaxies it is not present, and even turns into a weak *positive correlation*. The end result of using T04 metallicities is that the trends are no longer monotonic, which is inconsistent with the possibility that the M_*–Z–SFR relation is redshift invariant.[15]

To disentangle the effects of T04 sample selection that requires high S/N ratios in multiple lines from those that are intrinsic to the T04 metallicity method, we have also calculated the metallicities, using the exact methodology of T04, for galaxies that do not pass T04 cuts. Thus we arrive at the sample that is selected with only the S/N ratio cut on Hα line. Investigating the metallicity trends with such sample we still find (plots not shown) that T04 metallicities lead to much weaker trends against SSFR than M10 metallicities, but not so much to produce a drop at low SSFRs that would lead to non-monotonic behavior. This, apparently, is due to the additional bias of having S/N ratio selections in multiple lines.

Differences between M10 and T04 metallicities in the context of M_*–Z–SFR relation were previously noted by Yates et al. (2012), who ultimately preferred the T04 metallicities. Considering that most studies determine metallicities using simple methods similar to those used in M10 and not using the complicated Bayesian fitting of full emission line spectrum as in T04, it is important to understand if the simple method of M10 is at fault.

One concern regarding the M10 method is that it is based on semi-empirical calibrations (Maiolino et al. 2008). Maiolino et al. (2008) calibrate various individual line ratios of a sample of SDSS galaxies against the metallicities obtained from the theoretical calibrations of Kewley & Dopita (2002). Thus, such calibration will follow the theoretical models on *average*, but not necessarily for parts of the sample that have properties different from the average. Specifically, their calibrations may not be valid for galaxies that have ionization parameters that are very different from what is typical at a given line ratio value. To test the possibility that the M_*–Z–SFR relation based on M10 metallicities is affected by biases due to the variations of ionization parameter, we also calculate metallicities using the N2O2 method, which is the least sensitive to ionization parameter of all simple methods (methods that employ one ratio of lines; Kewley & Dopita 2002). We show the N2O2 metallicity versus SF trends in Figure 7(A), but now only for one mass bin ($\log M_* = 10.5$). The general sense of the trend is the same as it was with M10 metallicities: there is an anti-correlation for galaxies within the SF sequence, which becomes stronger above it. The overall slope is even slightly steeper than it was

[15] As explained in Section 2.3, for T04 metallicities we use medians of probability distribution functions. However, the results stay the same if averages or modes are used instead.

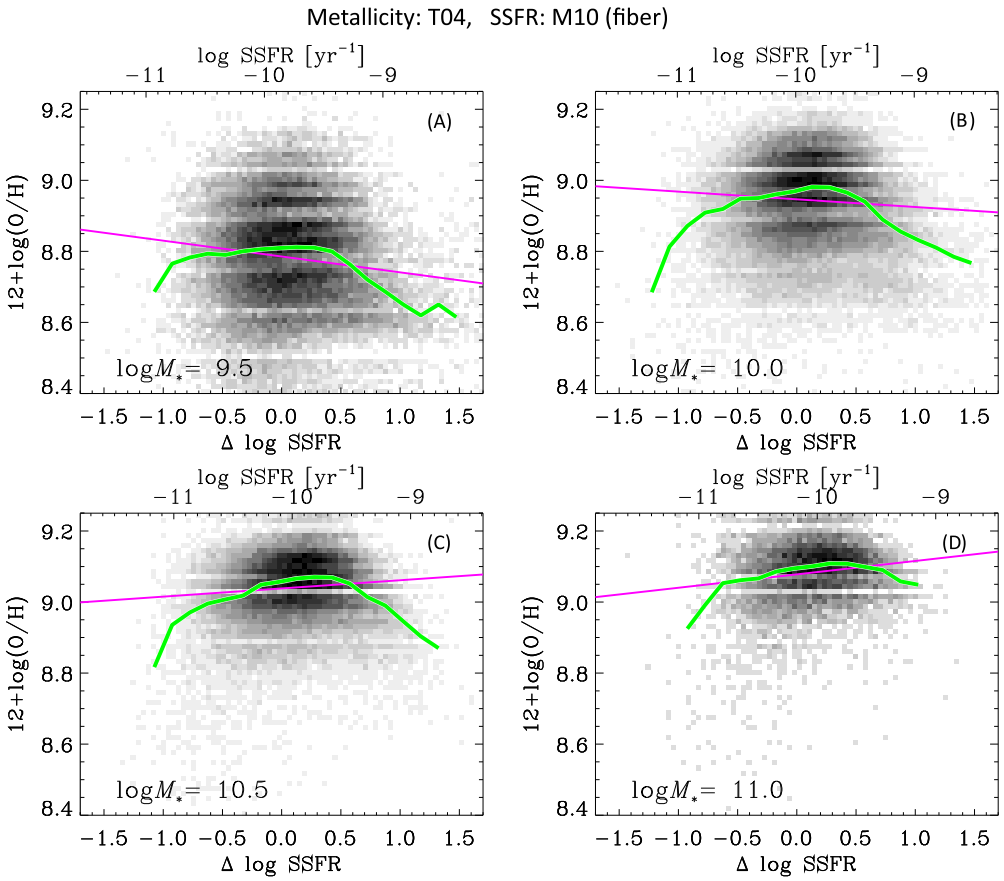

Figure 6. Dependence of metallicity on the offset from the star-forming sequence in different mass bins, where the metallicity is now from T04, while the SSFRs are still derived as in M10. A criterion required for M10 metallicities (that the estimates from N2 and R23 methods agree) is now dropped. Metallicity trends are weaker compared to those with M10 metallicities and are in some cases non-monotonic. This is a consequence of both the fact that T04 metallicities are only available for galaxies that have strong S/N ratios in multiple lines *and* that the T04 values yield weaker trends compared to those computed by M10.

(A color version of this figure is available in the online journal.)

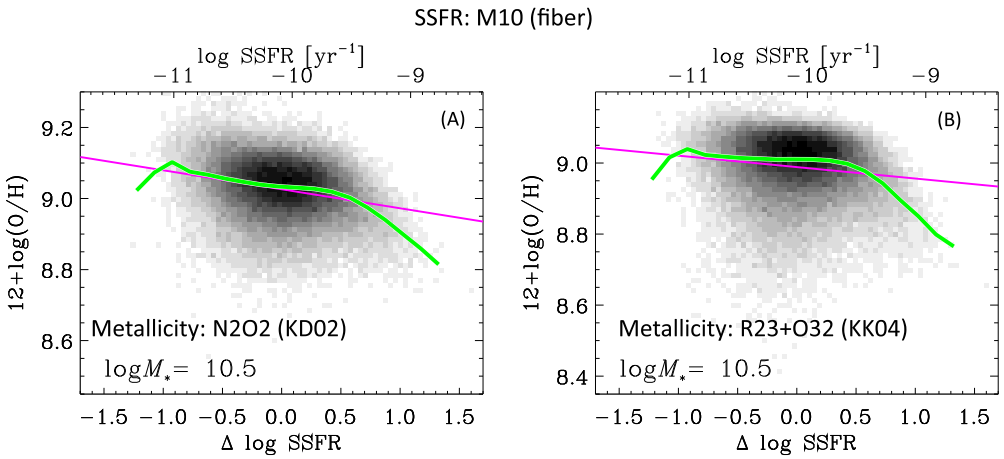

Figure 7. Dependence of metallicity on the offset from the star-forming sequence at $\log M_* = 10.5$, for two alternative metallicity methods. Panel (A) shows N2O2 metallicities calibrated according to Kewley & Dopita (2002), and panel (B) shows metallicities obtained with the Kobulnicky & Kewley (2004) "best" method of combining R23 with O32. Both methods should be less affected by the changes in the ionization parameter, and yet they show trends more similar to those based on M10 metallicities than based on T04 metallicities.

(A color version of this figure is available in the online journal.)

with M10 metallicities. There is no sign of flat or positively correlated trends as with T04 metallicities.

In their choice to adopt T04 metallicities as more fiducial, Yates et al. (2012) put forward an argument that any method for deriving metallicities involving nitrogen (such as M10's, which is an average of N2 and R23) is possibly affected by saturation. To address this concern, we now consider an oxygen-based (R23) calibration of Kobulnicky & Kewley (2004), which at the same time accounts for differences in the ionization parameter (through its dependence on O32). The results (again for $\log M_* = 10.5$ bin) are shown in Figure 7(B). While the median trend within the SF sequence is now somewhat weaker

than for either the M10 or N2O2 metallicities, they do not go away as in the case of T04 metallicities. In other mass bins (plots not shown), both the N2O2 and the R23+O32 trends are again closer to trends using M10 metallicities than those using T04 metallicities.

Based on the analysis presented in this section, we conclude that the use of T04 metallicities, even when accounting for the biases due to having multiple-line selections, produces SFR dependencies that are much smaller than those produced using conventional line ratio methods. It should be kept in mind that even among the methods that yield similar results, the strength of the dependence on (S)SFR will differ depending on the metallicity method and calibration (Andrews & Martini 2013). This reiterates the point that the comparisons of different samples must be based on same metallicity method and calibration (in addition to using comparable (S)SFR estimates, and allowing for non-linear trends, as emphasized in previous sections).

Furthermore, in this section we find that the dependence on SFR will depend on the S/N ratio cuts applied to the lines as discussed in de los Reyes et al. (2014). This is especially true for galaxies with lower (S)SFRs. This can be avoided by using a S/N ratio cut only on one hydrogen line (which can be made sufficiently high so that other lines are also well measured).

4. APPLICATION OF THE FRAMEWORK TO RESOLVE OPEN QUESTIONS

In this section, we apply the analysis framework presented in Section 3 to revisit some of the results regarding metallicity's secondary dependencies presented in recent literature. Specifically, we revisit the existence of another secondary parameter, galaxy size (Ellison et al. 2008), and also explore claims that the character of M_*–Z–SFR relation is different for galaxies of different mass (Yates et al. 2012; Lara-López et al. 2013), or the claims that the secondary dependence may be altogether spurious (Sánchez et al. 2013).

4.1. Is MZR Dependent on Galaxy Size?

The work that originally drew attention to the dependencies of MZR on other parameters, Ellison et al. (2008), claimed to have found not only MZR offsets due to SSFR, but also even *stronger* offsets resulting from galaxy physical sizes, in the sense that at a given mass larger galaxies have on average smaller metallicities. However, subsequent studies focused exclusively on the SFR aspect, neglecting the question of galaxy sizes, perhaps because the latter phenomenon had less clear intuitive interpretation, and because any result involving galaxy sizes in a sample where the physical scale and the fiber covering fraction span such wide ranges appears suspect. Furthermore, as pointed out by Ellison et al. (2008), simultaneous presence of both dependencies leads to the predictions that high-redshift MZRs should have much smaller evolution than what is observed, so the existence of a strong size dependence would potentially conflict with the basic idea of FMR—that it can account for MZR evolution.

Here we revisit the question of MZR's dependence on galaxy size by applying the methodology introduced in Section 3 (metallicity trends in 0.5 dex wide mass bins), but substituting SSFR with galaxy size. We use the same data for galaxy sizes (Simard et al. 2011) as used by Ellison et al. (2008), except that we take semimajor axis half-light radii in the g band (as opposed to r), based on single Sersic fits. The results for our augmented sample, and using M10 metallicities, are shown in Figure 8. Significant trends are seen in all mass bins, but they are stronger at lower masses. Bulk trends (purple fits) are not as strong as those versus SSFR, although they become more comparable at higher masses. The main difference is that the dependence versus SSFR has a two-mode behavior such that the trends above the SF sequence are much stronger, which results in the full range of median metallicities that is many times greater than the range of median metallicities due to the size dependence. For example, at $\log M_* = 9.5$ the total span of metallicities due to the size is $\sim$0.1 dex, while it is $\sim$0.5 dex with respect to the SSFR (Figure 4(A)). Interestingly, the trend versus size reverses for very large galaxies (half-light size $>$10 kpc), but there are very few such galaxies compared to those of smaller size.

One might have a concern that the size dependence is a just consequence of there being the primary dependence with SSFR. This would be the case if the size and SSFR were themselves strongly correlated in the sense that larger galaxies have higher SSFRs. However, this is not the case. We find (plots not shown) that the galaxies with higher SSFR on average have smaller sizes than galaxies with lower SSFRs (up to a factor of two). Furthermore, the dependence of metallicity on SSFR persists with the same intensity even when the galaxies are selected to lie in a very small range of physical sizes (plots not shown). Therefore, the two phenomena are independent. Finally, we confirm that the trends of metallicity with size remain when the sample is restricted to narrow redshift ranges (0.01), which demonstrates that the observed dependence is not an artifact of redshift-dependent covering fraction of the fibers.

The conclusion of this section is that the metallicity shows dependence on galaxy size that is independent from the dependence on SSFR and is not an artifact of aperture effects, nor of metallicity gradients within the galaxy (for the latter, see Ellison et al. 2008). However, the total trends are weaker compared to those with respect to SSFR, so one does not expect that the size dependence alone will produce much evolution in the MZR and thus affect the potential invariance of M_*–Z–SFR relation. Nevertheless, the size does appear to be a genuine contributing source of the dispersion (albeit small) in the MZR and is therefore in need of being tested with theoretical models.

4.2. Is There a Reversal in Z–SFR Anti-correlation at Higher Masses?

The character of the M_*–Z–SFR relation, that at a given mass there is an anti-correlation between SFR and metallicity, has been brought into question by Yates et al. (2012; and to some extent Lara-López et al. 2013), who find that this dependence *reverses* above $\log M_* \approx 10.2$, such that the higher (S)SFRs are associated with, on average, *higher* metallicities. Such result, if correct, would basically preclude the "fundamental" aspect of the FMR. Namely, as we go to higher redshifts, and SFRs at a given mass rise, one would expect, based on Yates et al. (2012) "reversal," that the metallicities of low mass galaxies would be offset lower compared to local galaxies (as observed) and that the metallicities of higher mass galaxies should on average be located *above* the local MZR. No such evolution of MZR has been reported in the current literature. So either the local relationship between Z, M_*, and SFR does not at all hold at other redshifts (is not fundamental), or there is a problem with the finding that there exists a reversal of trends.

Yates et al. (2012) found the reversal using T04 metallicities. They have also considered, but eventually decided not to trust, the metallicities determined according to the M10 method, which, even in their analysis, did not show any evidence of the reversal (their Figure 1). Our analysis (Section 3.5)

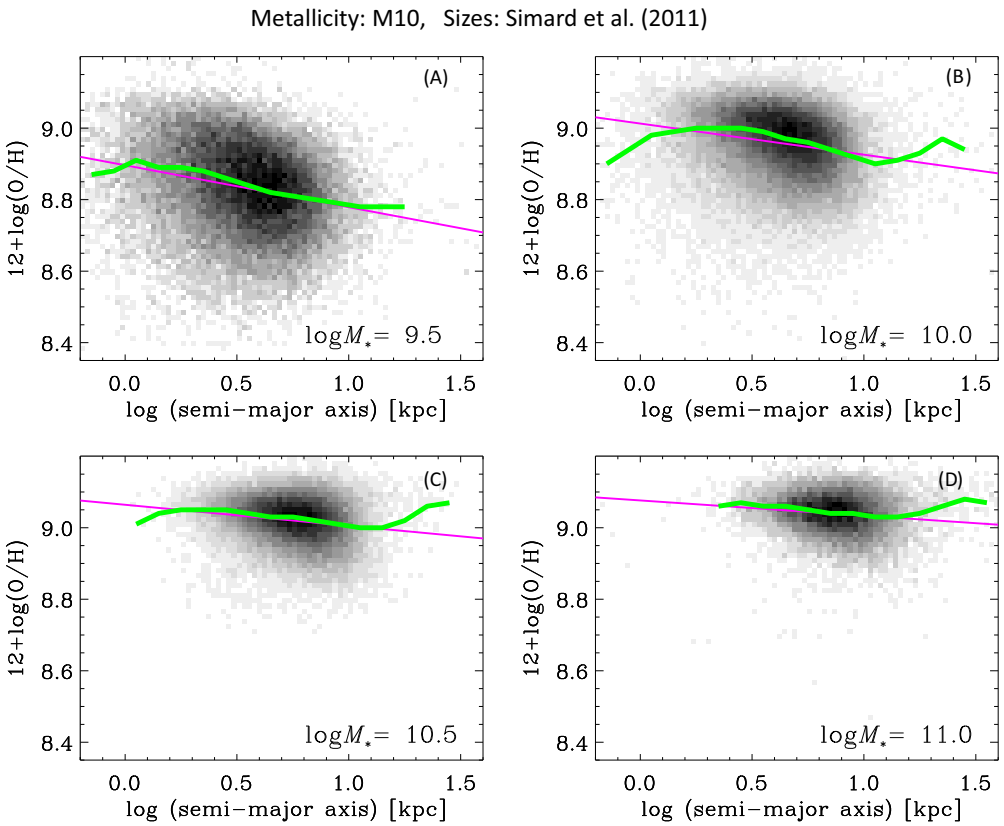

Figure 8. Dependence of metallicity on the galaxy size (half-light semi-major axis in the *g* band, in kiloparsecs) in different mass bins. Anti-correlations are present, but the overall trend in median metallicities is not as large as those with SSFR (Figure 4).

(A color version of this figure is available in the online journal.)

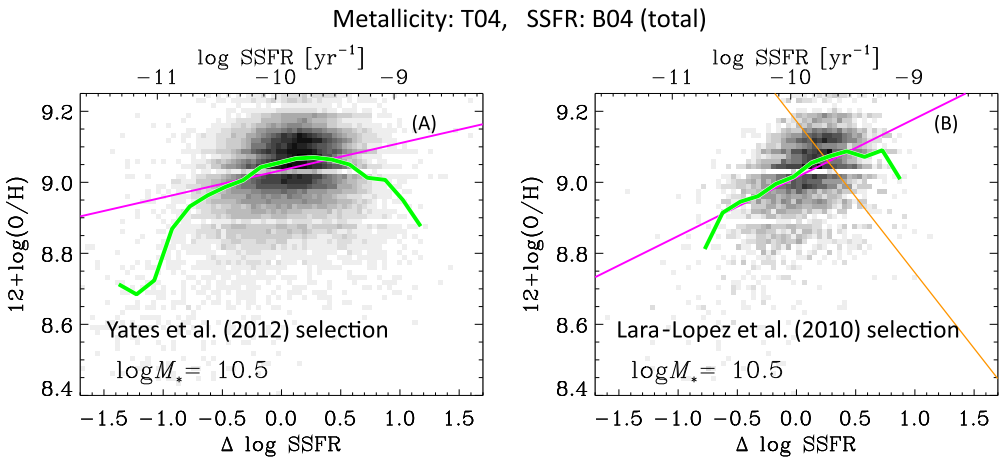

Figure 9. Dependence of metallicity on the offset from the star-forming sequence at $\log M_* = 10.5$, with samples selected as in Yates et al. (2012; panel (A)) and in Lara-López et al. (2010; panel (B)). Both studies utilize metallicities from T04 and total SFRs from B04. In panel (A) the overall trend shows a positive correlation between relative SSFR and metallicity, similar to that seen in our analysis of T04 metallicities (Figure 6(C)). However, this is the opposite behavior of the anti-correlation seen based upon other metallicity measures (Figures 4(C) and 7). Even stronger positive correlation in panel (B) can be traced to a lower redshift ceiling and higher S/N ratio cuts applied by Lara-López et al. (2010). However, this positive correlation is not captured by the Lara-López et al. (2010) "fundamental plane" parameterization of the relation (orange line), which, like the FMR of M10, implies that the galaxies follow an anti-correlation.

(A color version of this figure is available in the online journal.)

has shown that T04 metallicities intrinsically shows much weaker trends than other metallicity indicators, which are additionally exacerbated by T04 metallicities being available only for galaxies that fulfill S/N ratio criteria on multiple lines, leading to trends that are strongly non-monotonic, especially at higher masses (Figures 6(C) and (D)). Can this explain the results of Yates et al. (2012)? In Figure 9(A), we show metallicity versus SSFR for mass bin centered at $\log M_* = 10.5$, where, according to Yates et al. (2012), the reversal should already take place. The sample selection used in this figure follows that of Yates et al. (2012), applying S/N > 5 cuts in Hα, Hβ, and [N II]6584, redshift range of 0.005 to 0.25, and the requirement

that fiber captures at least 10% of the *r*-band flux. Yates et al. (2012) use aperture-corrected total SFR from B04.[16] Indeed, the general sense of the trend in Figure 9(A) (purple line) is one of a correlation (and therefore the reversal compared to the anti-correlation at lower masses). This is similar to what we have already seen when we discussed T04 metallicities (Figure 6), but with even fewer galaxies participating in the anti-correlation part of the trend, perhaps due to a different type of SFR or somewhat different sample cuts.

One could argue for reversal being real by noting that a similar effect may exist in trends of dust extinction versus SFR. Namely, Zahid et al. (2013) find that dust extinction A_V (estimated from the Balmer decrement) in SDSS shows an anti-correlation with SFR at lower masses, which turns into a positive correlation above $\log M_* > 10.2$. These trends are relatively weak and have a substantial scatter (∼0.5 mag). For SFR, Zahid et al. (2013) use B04 *total* SFRs. Interestingly, we confirm Zahid et al. (2013) results, but only when using total SSFRs. When we instead look at A_V versus *fiber* SSFR (either derived as in M10 or from B04), the mean trends have the same character irrespective of the mass: dust extinction rises with SSFR, reaches a peak, and then turns down above the SF sequence. The rising part of the trend becomes steeper with mass. Given that the Balmer decrement is determined in the fiber, it is more appropriate to compare it to the SSFR also measured in the fiber. Thus the results of Zahid et al. (2013) may not hold when the dust and the SSFR are measured in matching regions, possibly because the dust extinction and the SSFR do not scale alike.

T04 metallicities were also used in LL10, the other of the two papers that first reported the relationship between mass, SFR and metallicity. Like Yates et al. (2012), LL10 used total SFRs from B04, but also a much more restricted redshift range ($0.04 < z < 0.10$) and very high (>8) S/N ratio cuts in eight emission lines (four BPT lines, plus [O II]3726, 3729 and [S II]6717, 6731). We replicate LL10 selection and show the resulting metallicity versus SSFR plot at $\log M_* = 10.5$ in Figure 9(B). The apparent correlation ("reversal") is now even stronger than in Yates et al. (2012). This is the result of lower redshift range which preferentially eliminates less frequent high-SFR galaxies that would have added weight to the anti-correlation, and due to the high S/N ratio cuts that tend to preferentially remove low-SFR galaxies with high metallicities. LL10 do not discuss the reversal in their original paper, but do confirm it subsequently (Lara-López et al. 2013). However, it must be noted that the high-mass reversal is entirely at odds with the concept of the "fundamental plane" introduced by LL10. The sense of the fundamental plane is always one of anti-correlation. This can be seen in Figure 9(B), where we plot the locus of LL10 fundamental plane as the orange line (it is also evident in Figure 13 (top left panel) in Lara-López et al. 2013). Furthermore, the fundamental plane requires the slope κ to be mass-independent (e.g., Figure 13 (top left panel) in Lara-López et al. 2013), which is obviously not the case no matter which metallicity or SFR indicator is used. The fact that LL10 were able to derive the fundamental plane despite using T04 metallicities that cause the apparent reversal, is because the plane was constrained by more numerous lower mass galaxies that dominate in their sample and for which the general trend is that of anti-correlation, even using T04 metallicities (Figure 6(A)).

The conclusion is that the apparent reversal in metallicity versus (S)SFR, as seen in Yates et al. (2012), is primarily the result of using the available T04 metallicities, and would not be seen using other metallicity estimates (or even with T04 metallicities if they were available for a sample not biased by multiple-line S/N ratio cuts). Furthermore, the reversal would have conflicted with the fundamental aspect of the local Z–M_*–SFR relation because it would no longer be able to explain the MZR evolution.

4.3. Is M_*–Z–SFR Relation Merely an Artifact of Aperture Effects?

One potentially serious limitation of all studies of the relationships between metallicity, mass, and SFR that are based on SDSS data is that the metallicity measurements come from fiber spectroscopy, which covers part of the galaxy in a way that is redshift and galaxy-size dependent. Sánchez et al. (2013) made efforts to address this concern by observing a sample of 150 local ($z < 0.03$) galaxies using an integral field spectrograph PMAS/PPAK mounted on Calar Alto 3.5 m as part of the CALIFA survey. In addition to the measurements of resolved H II regions, Sánchez et al. (2013) determine global estimates for galaxy metallicity in a physically motivated way (at one effective radius), as well as the total SFRs based on Hα. Such a sample, even though relatively small but being free from aperture effects, could prove essential in either strengthening or weakening the status of the M_*–Z–SFR relation. The analysis performed on global measures by Sánchez et al. (2013) concluded that no dependence of MZR on SFR existed. Furthermore, they tentatively explained the apparent presence of this dependence in SDSS data to be due to the aperture affects (their Appendix).

Here we reanalyze Sánchez et al. (2013) data using our preferred methodology: metallicity versus relative SSFR in individual mass bins. The results are shown in Figure 10. Except in the lowest mass bin (panel (A)), the anti-correlation between metallicity (determined by Sánchez et al. 2013 using Pettini & Pagel 2004 calibration of O3N2 method) and SSFR (i.e, the offset from the SF sequence as derived with Sánchez et al. 2013 data) is convincingly present (purple lines show linear unweighted fits). In mass bins centered at $\log M_* = 10.0$ and 10.5, there is only a 5% and 3% probability that the anti-correlation is due to chance (obtained using bootstrap resampling; similar results, 3% and 0.1%, are obtained when measurements are perturbed within the error bars). The positive correlation in the lowest mass bin is not statistically significant (there is a 37% probability that it is due to chance), but it is incompatible with very strong anti-correlation expected at those masses. We point out that Sánchez et al. (2013) sample is incomplete at those masses, and the apparent lack of anti-correlation could potentially be due to the apparent size selection present in CALIFA data set (Walcher et al. 2014). We believe that the reason why this dependence was not detected in the analysis of Sánchez et al. (2013) was because the sample was not split by stellar mass (their Figure 4, bottom right panel). Furthermore, in a small sample that lacks extreme star formers, the trend in metallicities will be relatively modest and therefore difficult to spot on a mass–metallicity plot color-coded by SFR (their Figure 4, lower left panel).

We conclude that it is very encouraging that the measurements that avoid the issues of SDSS fibers confirm the MZR

[16] B04 total SFRs combine the SFR determined in the fiber (Section 2.3) with the SFR estimated for the region outside of the fiber. These outer-ring SFRs were based on outer broadband optical fluxes, calibrated to match the SFRs of fibers having the same color. As such, the total B04 SFRs are emission-line/broadband hybrids.

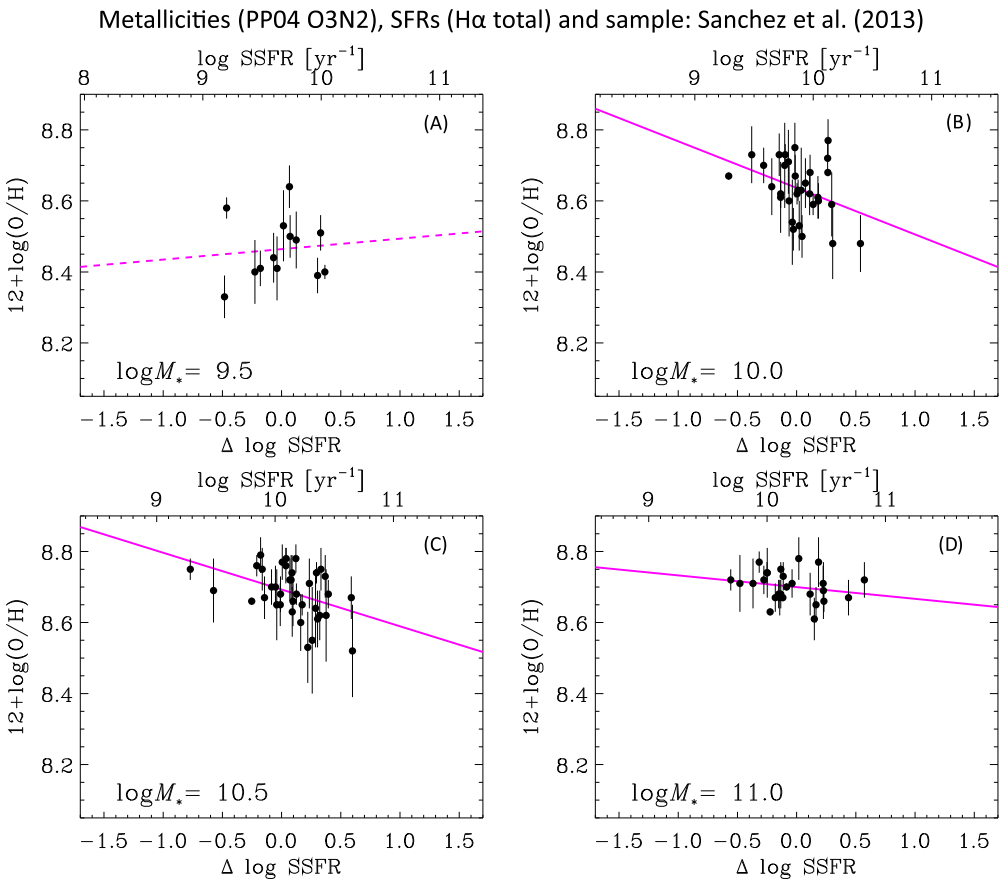

Figure 10. Dependence of metallicity on the offset from the star-forming sequence for the CALIFA sample of Sánchez et al. (2013). Sánchez et al. (2013) observed 150 galaxies with integral field spectroscopy and were therefore able to derive metallicities and SFRs that better reflect entire galaxies than SDSS fiber measures and should not be susceptible to potential aperture biases. Interestingly, we find that (except in the lowest mass bin, panel (A)) statistically significant anti-correlations (purple lines show unweighted linear fits) are present, with strengths that are comparable to those in SDSS sample.

(A color version of this figure is available in the online journal.)

dependence on SSFR, and in a degree that is comparable to that using more extensive SDSS data.

5. DISCUSSION: IMPLICATIONS FOR THEORETICAL STUDIES

Chemical enrichment of galaxies and its change through cosmic time is the result of an intricate interplay between star formation (turning gas into stars), stellar evolution (releasing enriched gas into the ISM), regulation of SF (different forms of feedback), galaxy-scale outflows (possibly related to feedback processes), as well as gas accretion (from intergalactic medium (IGM), recycled outflow gas, or from gas-rich mergers). Each of these individual processes are themselves not fully understood.

There are two main aspects of chemical enrichment: that of the stars, and of the ISM (typically of gas in photo-ionized H II regions)). Both are usually expressed in terms of a metallicity. Stellar metallicities are more representative of the sum record of the history of metal enrichment, while gas metallicities are more reflective of the current level of chemical enrichment. The study of stellar metallicities of individual galaxies requires good absorption-line spectroscopy, hence it is mostly limited to low redshifts (Gallazzi et al. 2005), with pioneering efforts at intermediate and high redshifts currently under way (Sommariva et al. 2012; Gallazzi et al. 2014).

Theoretical efforts first focused on trying to reproduce the local MZR and its evolution with redshift, and were only more recently modified to address the dependence on SFR. In principle, the existence of MZR can be explained in the context of a closed-box model, simply as the consequence of "downsizing," a scenario in which more massive galaxies have produced most of their stars and metals early in the history of the universe (e.g., Garnett 2002; Savaglio et al. 2005). However, simple closed-box scenarios violate numerous constraints, including Milky Way G- and M-dwarf metallicities (e.g., Woolf & West 2012). Thus, building on early ideas by Dekel & Silk (1986), T04 proposed a model in which galactic winds (outflows), which are responsible for the removal of metal-rich gas from SF regions, are more efficient in low-mass galaxies, leading to the observed MZR. More recent analytic models typically require both inflow and outflow to match galaxy metallicities (e.g., Dalcanton 2007; Peeples & Shankar 2011).

Hydrodynamic galaxy formation simulations that include strong feedback have been able to reproduce the MZR. Brooks et al. (2007) used high-resolution zoom disk galaxy simulations to argue that the MZR faint-end slope is primarily set by the lowered efficiency of converting gas into stars in the ISM (due to supernova feedback), as opposed to ejecting metals. Finlator & Davé (2008) and Davé et al. (2011) used lower-resolution cosmological simulations to argue that outflows lowered the efficiency of converting infalling (not ISM) gas into stars, and Davé et al. (2012) showed that this can be effectively parameterized in a simple analytic framework that predicts

$Z \propto \eta^{-1}$ in small galaxies, where η is the mass loading factor. The observed faint-end MZR of $Z \propto M_*^{0.3-0.4}$ then implies $\eta \propto M_*^{-1/3}$, consistent with momentum-driven winds (Murray et al. 2005; Oppenheimer & Davé 2008). More recent cosmological simulations favor a steeper scaling of η to reproduce the stellar mass function, but this results in an MZR that is too steep (Davé et al. 2013). Overenriching outflows, as suggested by data (e.g., Heckman et al. 2000) makes the problem worse, and indeed the Illustris simulation employs *under*enriched outflows, which is difficult to justify physically but improves agreement with data (Vogelsberger et al. 2014). Recent zoom simulations that include H_2-based star formation can reproduce the MZR and stellar mass data via a combination of outflows driving out gas and metals together with a reduced ISM star formation efficiency owing to lower metallicities (L. Christensen et al. 2015, in preparation). Clearly the physics that sets the MZR shape is not fully sorted, but successful models commonly invoke increasingly stronger outflows to low-masses, with saturation at high masses where outflows become ineffective. Regarding the MZR evolution, outflows are necessary to explain slow enrichment by $z \sim 2$ (Finlator & Davé 2008), but the overall increase of metallicity at a given mass is due to the accreted gas becoming more metal rich (Davé et al. 2011).

Cosmological simulations concurrently predict the M_*–Z–SFR relation. Davé et al. (2011) showed that projecting the simulated galaxies onto the FMR plane of M10 indeed lowered the scatter, though not by quite as much as expected from M10. The trend qualitatively arises in these models because pristine infall both increases the gas content to stimulate star formation, while reducing the gas-phase metallicity. Galaxies thus fluctuate around the "equilibrium" MZR owing to fluctuations in the infall rate (such as mergers). Finlator & Davé (2008) showed that the MZR scatter is thus set by the timescale to return to the "equilibrium" MZR, and in simulations when this dilution timescale became greater than the halo dynamical time, the MZR scatter blew up. Such ideas were encapsulated in the analytic "gas regulator" model of Lilly et al. (2013), in which the metallicity is determined instantaneously by gas consumption timescale (ϵ), mass loading of wind outflow (λ), and the specific SFR. The M_*–Z–SFR relation emerges in this model if ϵ and λ are mass-dependent. Furthermore, in gas regulator model the M_*–Z–SFR relation is redshift-invariant if ϵ and λ are themselves constant with time. The model of Lilly et al. (2013) was generalized by Pipino et al. (2014) to allow for an evolving efficiency of SFR from inflowing gas, and was thus able to provide a very good match to both the MZR and the M_*–Z–SFR relation. Zahid et al. (2014a) forwarded a related empirical model in which gas infall dilutes the existing metallicity, and hence argued the MZR evolution is fundamentally governed by a relation between metallicity and gas-to-stellar mass ratio. However, inflow fluctuations are not the only viable explanation. Dayal et al. (2013) suggested instead that the M_*–Z–SFR relation arises because higher SFR galaxies have stronger outflows that eject more metals. A review of recent theoretical ideas related to gas accretion and its impact on the MZR can be found in Sanchez Almeida et al. (2014).

Results of our study have a number of implications for theoretical efforts. We have seen that the exact character of M_*–Z–SFR relation will change depending on the metallicity, and to some extent, the SFR indicator. Therefore, theoretical results should not be expected to reproduce details of any empirical relation, but instead should lie in the range of empirical estimates. The strength of the correlations will be affected by the accuracy of measured quantities, in particular the ability to accurately identify galaxies with high SFRs. Therefore, it is recommended that the results of simulation also include realistic effects of observational errors. In the same way, the mass-binned metallicity versus SSFR plots were shown to be a useful framework to characterize the M_*–Z–SFR relation empirically, so it is a recommended way to show theoretical predictions and compare them to the observations.

Our results further challenge models to produce not only the dependence on SFR, but also make it stronger for lower-mass galaxies. Also, what we find to be a consistent feature among galaxies of $\log M_* \lesssim 10.5$ is the change in strength of SFR-dependence above the SF sequence. Theoretical work has yet to address this. Our suggestion is that it reflects the change in the mode of star-formation above the SF sequence, possibly in relation to galaxy interactions. If mergers are common in this regime, one expects lower metallicities (and therefore stronger Z–SSFR trends) simply due to the progenitor bias. Note that a late-stage 1:1 major merger with the final mass $\log M_* = 10$ will still have the metallicity of a $\log M_* = 9.7$ galaxy because it hasn't had time to enrich its gas yet. The factor of two in mass around $\log M_* = 9.7$ corresponds to roughly a 0.1 dex shift in metallicity (e.g., Figure 2), which would explain a some of the difference between purple and green lines in Figure 4(B).

Finally, we confirm that the dependence of metallicity on galaxy size is real and independent of the trends with SFR. One possibility is that the galaxies that are larger than what is typical for their mass are undergoing higher rates of accretion onto the disk, which is then reflected in the overall reduction of the metallicity.

6. CONCLUSIONS

The aim of this work was to establish a more physically motivated non-parametric framework for the study of the M_*–Z–SFR relation, and to apply the methodology to understand the origins of conflicting results regarding the characterization of the local relation. We demonstrate that such a non-parametric framework is needed to accurately determine whether the MZR has secondary dependencies on other parameters, and whether local and higher-redshift samples can be described with a single "fundamental" metallicity relation. Here, we have sought to provide a more coherent picture of the empirical properties of the local M_*–Z–SFR relation and summarize our results as follows.

1. A more physically motivated second parameter for the M_*–Z relation is the *relative specific* SFR, i.e., the level of star formation compared to what is typical for a galaxy of that mass, rather than the *absolute* (S)SFR. The relative SSFR represents the offset from the star-forming sequence (the "main sequence") along the SSFR axis. Selection of galaxies with high relative SSFR better mimics high-redshift selection. The use of *specific* SFR as opposed to SFR also has the advantage that the measurement of star formation within SDSS spectroscopic fibers is physically meaningful, since it represents the intensity of star formation in the same region where the metallicity is measured. We caution that absolute fiber SFRs, which were used in the Mannucci et al. (2010) formulation of FMR, are strongly distance-dependent and cover an average of only 25% of the total SFR.
2. Following from conclusion 1, our preferred framework for the study of M_*–Z secondary dependencies and for investigating whether the same trends apply at different redshifts (i.e., the FMR) consists of plotting the

metallicity against the relative SSFR as an independent parameter, but restricted to galaxies of a certain, relatively narrow mass range (0.2–0.5 dex) at a time. This method is free from assumptions of the parameterization of M_*–Z–SFR relation and exposes important details of the relationship that are not captured by previous parameterizations (e.g., a plane or projection of minimal scatter; see conclusions 3, 4, 5; de los Reyes et al. 2014). All figures in this paper, beginning with Figure 4, apply and illustrate this method.

3. We confirm that metallicity's dependence on SSFR is weaker for more massive galaxies, becoming very weak or absent above $\log M_* \approx 10.5$ (Ellison et al. 2008).
4. The secondary dependence on SSFR has a markedly different character for intense star formers (with SSFR $\gtrsim$ 0.6 dex above the star-forming sequence) than for "normal" star-forming galaxies (those in the core or below the sequence). The trend indicates a possible two-mode behavior, which can be parameterized with a broken linear fit of 12+log(O/H) versus log SSFR, with slopes, $\kappa_{\rm high}$ and $\kappa_{\rm low}$. The galaxies above the SF sequence have a much stronger dependence on the SSFR, which notably have similar $\kappa_{\rm high}$ regardless of the mass. However, as the mass increases, a smaller and smaller percentage of galaxies belongs to this group of high SSFR galaxies.
5. Conclusion 4 implies that characterizing the relation between mass, metallicity, and SFR with a flat plane (Lara-López et al. 2010, 2013) or with a projection that minimizes the scatter (Equation (5) of Mannucci et al. 2010) forces the trends to be identical at different masses and/or at different SSFRs, which is not the case. The use of such descriptions of the local M_*–Z–SFR relation, which would be dominated by weaker trends of the majority of local galaxies, could lead to incorrect predictions for high-redshift samples, off by 0.2 dex or more in metallicity (Maier et al. 2014).
6. Contrary to common wisdom, accounting for SSFR dependence has a modest effect on the reduction of scatter in metallicities—it is, at most, 20% at the lowest masses and down to 0% at higher masses, confirming the results of Ellison et al. (2008). This is in contrast to the reduction of the scatter of median-binned values, which is more dramatic (Mannucci et al. 2010). In other words, the M_*–Z–SFR relation cannot be thought of as a thin surface. Furthermore, the remaining scatter is still higher than the formal metallicity measurement errors, suggesting that other parameters may be more closely related to metallicity than the (S)SFR.
7. For the majority of galaxies that do not have very high SSFRs, the strength of metallicity's dependence on SSFR ($\kappa_{\rm low}$) is similar when using fiber SSFRs (based on emission lines, particularly Hα) or the total SSFRs (based on integrated fluxes), eliminating concerns that the SFR dependence is due to a spurious correlation between metallicity and emission-line based SFR. For intense star-formers ($\gtrsim$0.6 dex above the star-forming sequence), Hα SSFRs produce stronger trends than mid-IR SSFRs, which could due to the shorter timescales that Hα is sensitive to, or the fact that it measures SFR in the same region in which the metallicity is measured (fiber).
8. The character and the strength of trends of metallicity versus SSFR are sensitive to signal-to-noise ratio selection cuts applied to the emission lines. The least biased method is to only select on the S/N of a single Balmer line. To ensure that usable metallicity estimates are obtained, this cut can be relatively high (Mannucci et al. 2010). Applying cuts to multiple lines preferentially removes high-metallicity galaxies with lower SSFRs, effectively leading to weaker metallicity trends (de los Reyes et al. 2014).
9. The choice of metallicity indicator affects the strength of the Z versus SSFR trends, but an anti-correlation is always observed: higher SFRs at a given mass on average have lower metallicities. The exception is for metallicities derived using the method of Tremonti et al. (2004, T04), which show non-monotonic behavior, with average metallicities decreasing both above and below the SF sequence, especially at higher masses. The behavior arises both from the signal-to-noise ratio cuts applied to multiple lines for which T04 metallicities are available (conclusion 8), and from the fact that T04 values yield weaker metallicity trends. More work is needed to establish the root causes of such differences with respect to other methods. The "reversal" reported in some recent studies, i.e., that the trend of metallicity versus (S)SFR becomes *positively* correlated for high-mass galaxies can be attributed to the use of T04 metallicities in these studies. The reversal is not consistent with the concept on an FMR as it would predict that the high-redshift MZRs are offset below the local MZRs at low mass and offset *above* the local MZRs at high mass.
10. Application of our methodology shows that the dependence of metallicity on SSFR is present in the CALIFA data set, which is based on integral field spectroscopy for local galaxies, whereas Sánchez et al. (2013) reported no significant secondary dependence on SFR and concluded that the M_*–Z–SFR relation is an artifact of spectroscopy aperture biases. We show that the CALIFA data have a dependence on the SSFR that is broadly consistent with the relation followed by galaxies in the SDSS, except at the lowest masses, where the available CALIFA data are few and show no clear dependence.
11. We confirm that metallicity has a secondary dependence on galaxy size (half-light semimajor axis), as originally found by Ellison et al. (2008), and that it is independent of the dependence on (S)SFR and also not the result of aperture effects. At masses above $\log M_* \gtrsim 10$, the strength of this correlation is similar to the dependence with respect to SSFR, but the total extent of the median metallicities due to the galaxy size is smaller than that due to SSFR. The end result is that the dependence on galaxy size is secondary to that on SSFR and is therefore less relevant in the evolutionary context, but still in need of a theoretical explanation.

The non-parametric analysis framework presented here will be used to evaluate whether the relation defined in the local universe by SDSS galaxies also describes galaxies at higher redshift (i.e., whether it is "fundamental") in future work (S. Salim et al. 2015, in preparation).

We gratefully acknowledge efforts to design, construct and operate SDSS, *GALEX* and *WISE*, and produce and disseminate their data products. This work was supported through NASA ADAP award NNX12AE06G. We thank Steven Janowiecki for his help in assembling some of the data sets and Molly Peeples, Robert Yates and Liese van Zee for discussions regarding their work.

REFERENCES

Andrews, B. H., & Martini, P. 2013, ApJ, 765, 140
Baldwin, J. A., Phillips, M. M., & Terlevich, R. 1981, PASP, 93, 5
Belli, S., Jones, T., Ellis, R. S., & Richard, J. 2013, ApJ, 772, 141
Brinchmann, J., Charlot, S., White, S. D. M., et al. 2004, MNRAS, 351, 115
Brooks, A. M., Governato, F., Booth, C. M., et al. 2007, ApJL, 655, L17
Bruzual, G., & Charlot, S. 2003, MNRAS, 344, 1000
Calzetti, D. 2013, Secular Evolution of Galaxies (Cambridge: Cambridge Univ. Press), 419
Calzetti, D., Armus, L., Bohlin, R. C., et al. 2000, ApJ, 533, 682
Cardelli, J. A., Clayton, G. C., & Mathis, J. S. 1989, ApJ, 345, 245
Charlot, S., & Fall, S. M. 2000, ApJ, 539, 718
Christensen, L., Richard, J., Hjorth, J., et al. 2012, MNRAS, 427, 1953
Cowie, L. L., & Barger, A. J. 2008, ApJ, 686, 72
Cresci, G., Mannucci, F., Sommariva, V., et al. 2012, MNRAS, 421, 262
Cullen, F., Cirasuolo, M., McLure, R. J., Dunlop, J. S., & Bowler, R. A. A. 2014, MNRAS, 440, 2300
da Cunha, E., Charlot, S., & Elbaz, D. 2008, MNRAS, 388, 1595
Dalcanton, J. J. 2007, ApJ, 658, 941
Dale, D. A., & Helou, G. 2002, ApJ, 576, 159
Davé, R., Finlator, K., & Oppenheimer, B. D. 2011, MNRAS, 416, 1354
Davé, R., Finlator, K., & Oppenheimer, B. D. 2012, MNRAS, 421, 98
Davé, R., Katz, N., Oppenheimer, B. D., Kollmeier, J. A., & Weinberg, D. H. 2013, MNRAS, 434, 2645
Dayal, P., Ferrara, A., & Dunlop, J. S. 2013, MNRAS, 430, 2891
Dekel, A., & Silk, J. 1986, ApJ, 303, 39
de los Reyes, M., Ly, C., Lee, J. C., et al. 2014, AJ, in press
Elbaz, D., Dickinson, M., Hwang, H. S., et al. 2011, A&A, 533, AA119
Ellison, S. L., Patton, D. R., Simard, L., & McConnachie, A. W. 2008, ApJL, 672, L107
Erb, D. K., Shapley, A. E., Pettini, M., et al. 2006, ApJ, 644, 813
Finlator, K., & Davé, R. 2008, MNRAS, 385, 2181
Gallazzi, A., Bell, E. F., Zibetti, S., Brinchmann, J., & Kelson, D. D. 2014, ApJ, 788, 72
Gallazzi, A., Charlot, S., Brinchmann, J., White, S. D. M., & Tremonti, C. A. 2005, MNRAS, 362, 41
Garnett, D. R. 2002, ApJ, 581, 1019
Heckman, T. M., Lehnert, M. D., Strickland, D. K., & Armus, L. 2000, ApJS, 129, 493
Henry, A., Scarlata, C., Domínguez, A., et al. 2013, ApJL, 776, L27
Hoopes, C. G., Heckman, T. M., Salim, S., et al. 2007, ApJS, 173, 441
Juneau, S., Bournaud, F., Charlot, S., et al. 2014, ApJ, 788, 88
Kauffmann, G., Heckman, T. M., Tremonti, C., et al. 2003, MNRAS, 346, 1055
Kennicutt, R. C., & Evans, N. J. 2012, ARA&A, 50, 531
Kennicutt, R. C., Jr. 1998, ARA&A, 36, 189
Kewley, L. J., & Dopita, M. A. 2002, ApJS, 142, 35
Kewley, L. J., Dopita, M. A., Leitherer, C., et al. 2013, ApJ, 774, 100
Kewley, L. J., & Ellison, S. L. 2008, ApJ, 681, 1183
Kobulnicky, H. A., & Kewley, L. J. 2004, ApJ, 617, 240
Lamareille, F., Brinchmann, J., Contini, T., et al. 2009, A&A, 495, 53
Lara-López, M. A., Cepa, J., Bongiovanni, A., et al. 2010, A&A, 521, L53
Lara-López, M. A., Hopkins, A. M., López-Sánchez, A. R., et al. 2013, MNRAS, 434, 451
Lee, J. C., Gil de Paz, A., Kennicutt, R. C., Jr., et al. 2011, ApJS, 192, 6
Lee, J. C., Gil de Paz, A., Tremonti, C., et al. 2009, ApJ, 706, 599
Lee, J. C., Salzer, J. J., & Melbourne, J. 2004, ApJ, 616, 752
Lequeux, J., Peimbert, M., Rayo, J. F., Serrano, A., & Torres-Peimbert, S. 1979, A&A, 80, 155
Lilly, S. J., Carollo, C. M., Pipino, A., Renzini, A., & Peng, Y. 2013, ApJ, 772, 119
Ly, C., Malkan, M. A., Nagao, T., et al. 2014, ApJ, 780, 122
Maier, C., Lilly, S. J., Ziegler, B., et al. 2014, ApJ, 792, 3
Maiolino, R., Nagao, T., Grazian, A., et al. 2008, A&A, 488, 463
Magdis, G. E., Daddi, E., Béthermin, M., et al. 2012, ApJ, 760, 6
Mannucci, F., Cresci, G., Maiolino, R., Marconi, A., & Gnerucci, A. 2010, MNRAS, 408, 2115
Marcillac, D., Elbaz, D., Chary, R. R., et al. 2006, A&A, 451, 57
Martin, D. C., Seibert, M., Buat, V., et al. 2005, ApJL, 619, L59
McGaugh, S. S. 1991, ApJ, 380, 140
Murray, N., Quataert, E., & Thompson, T. A. 2005, ApJ, 618, 569
Nagao, T., Maiolino, R., & Marconi, A. 2006, A&A, 459, 85
Nakajima, K., & Ouchi, M. 2014, MNRAS, 442, 900
Oppenheimer, B. D., & Davé, R. 2008, MNRAS, 387, 577
Pagel, B. E. J., Edmunds, M. G., Blackwell, D. E., Chun, M. S., & Smith, G. 1979, MNRAS, 189, 95
Peeples, M. S., & Shankar, F. 2011, MNRAS, 417, 2962
Peeples, M. S., & Somerville, R. S. 2013, MNRAS, 428, 1766
Pérez-Montero, E., Contini, T., Lamareille, F., et al. 2013, A&A, 549, A25
Pettini, M., & Pagel, B. E. J. 2004, MNRAS, 348, L59
Pipino, A., Lilly, S. J., & Carollo, C. M. 2014, MNRAS, 441, 1444
Richard, J., Jones, T., Ellis, R., et al. 2011, MNRAS, 413, 643
Rodighiero, G., Daddi, E., Baronchelli, I., et al. 2011, ApJL, 739, LL40
Salim, S., Dickinson, M., Rich, R. M., et al. 2009, ApJ, 700, 161
Salim, S., & Lee, J. C. 2012, ApJ, 758, 134
Salim, S., Rich, R. M., Charlot, S., et al. 2007, ApJS, 173, 267
Salzer, J. J., Lee, J. C., Melbourne, J., et al. 2005, ApJ, 624, 661
Sánchez, S. F., Rosales-Ortega, F. F., Jungwiert, B., et al. 2013, A&A, 554, A58
Sanchez Almeida, J., Elmegreen, B. G., Munoz-Tunon, C., & Elmegreen, D. M. 2014, A&ARv, 22, 71
Savaglio, S., Glazebrook, K., Le Borgne, D., et al. 2005, ApJ, 635, 260
Schiminovich, D., Wyder, T. K., Martin, D. C., et al. 2007, ApJS, 173, 315
Simard, L., Mendel, J. T., Patton, D. R., Ellison, S. L., & McConnachie, A. W. 2011, ApJS, 196, 11
Sommariva, V., Mannucci, F., Cresci, G., et al. 2012, A&A, 539, A136
Speagle, J. S., Steinhardt, C. L., Capak, P. L., & Silverman, J. D. 2014, ApJS, 214, 15
Steidel, C. C., Rudie, G. C., Strom, A. L., et al. 2014, ApJ, 795, 165
Stott, J. P., Sobral, D., Bower, R., et al. 2013, MNRAS, 436, 1130
Strauss, M. A., Weinberg, D. H., Lupton, R. H., et al. 2002, AJ, 124, 1810
Tremonti, C. A., Heckman, T. M., Kauffmann, G., et al. 2004, ApJ, 613, 898
Troncoso, P., Maiolino, R., Sommariva, V., et al. 2014, A&A, 563, A58
van Zee, L., Haynes, M. P., & Salzer, J. J. 1997, AJ, 114, 2497
Vogelsberger, M., Genel, S., Springel, V., et al. 2014, MNRAS, 444, 1518
Walcher, C. J., Wisotzki, L., Bekeraité, S., et al. 2014, A&A, 569, A1
Woo, J., Dekel, A., Faber, S. M., et al. 2013, MNRAS, 428, 3306
Woolf, V. M., & West, A. A. 2012, MNRAS, 422, 1489
Wright, E. L., Eisenhardt, P. R. M., Mainzer, A. K., et al. 2010, AJ, 140, 1868
Wuyts, E., Kurk, J., Förster Schreiber, N. M., et al. 2014, ApJL, 789, L40
Wuyts, E., Rigby, J. R., Sharon, K., & Gladders, M. D. 2012, ApJ, 755, 73
Yabe, K., Ohta, K., Iwamuro, F., et al. 2014, MNRAS, 437, 3647
Yates, R. M., Kauffmann, G., & Guo, Q. 2012, MNRAS, 422, 215
Yuan, T.-T., Kewley, L. J., & Richard, J. 2013, ApJ, 763, 9
Zahid, H. J., Kewley, L. J., & Bresolin, F. 2011, ApJ, 730, 137
Zahid, H. J., Bresolin, F., Kewley, L. J., Coil, A. L., & Davé, R. 2012, ApJ, 750, 120
Zahid, H. J., Dima, G. I., Kudritzki, R.-P., et al. 2014a, ApJ, 791, 130
Zahid, H. J., Kashino, D., Silverman, J. D., et al. 2014b, ApJ, 792, 75
Zahid, H. J., Yates, R. M., Kewley, L. J., & Kudritzki, R. P. 2013, ApJ, 763, 92